THE DISCOVERY OF THE TOP QUARK

PEKKA K. SINERVO
Department of Physics, University of Toronto,
Toronto, Ontario, Canada M5S 1A7

1 Introduction

1.1 The Case for Top

The top quark and the Higgs boson are the heaviest elementary particles predicted by the standard model. The four lightest quark flavours, the up, down, strange and charm quarks, were well-established by the mid-1970's. The discovery in 1977 [1] of the Υ resonances, a new family of massive hadrons, required the introduction of the fifth quark flavour. Experimental and theoretical studies have indicated that this quark also has a heavier partner, the top quark.

Indirect evidence for the top quark comes from a number of sources. The most compelling data come from the observed properties of the scattering process $e^+e^- \to b\bar{b}$, where the asymmetry in the scattering of the b quark relative to the incoming electron direction implies that the b quark has weak isospin of 0.5. The most precise measurement of this comes from the LEP collider, where this asymmetry has been measured[2] to be 0.097 ± 0.004, in excellent agreement with the standard model expectation of 0.100 assuming that the b quark is a member of an $SU(2)$ doublet. The other member of that doublet would by definition be the top quark.

Additional indirect evidence comes from the study of b quark decays. It has been experimentally determined that the b quark does not decay via processes that yield zero net flavour in the final state (*e.g.*, $b \to \mu^+\mu^- X$), or where the decay results in only a quark of the same charge (*e.g.*, $b \to sX$ where X is a state with no net flavour quantum numbers) [3]. The absence of these "flavour-changing neutral currents" in the standard model imply that the b quark is a member of an $SU(2)$ doublet.

Finally, evidence for the existence of a massive fermion that couples via the electroweak force to the b quark comes from detailed measurements of the Z and W bosons performed at LEP, SLC, the CERN S$p\bar{p}$S and the Fermilab Tevatron Collider. This body of data, and in particular the radiative mass shifts of the electroweak bosons, can only be described in the standard model by introducing a top quark. A recent compilation of data [4] indicates that the standard model top quark has a mass of

$$M_{top} = 169^{+16\ +17}_{-18\ -20}\ \mathrm{GeV/c^2}. \tag{1}$$

The second uncertainty corresponds to variations of the unknown Higgs boson mass between 60 and 1000 GeV/c^2 (its nominal value is 300 GeV/c^2).

Taken together, these observations make a strong case for the top quark's existence. They also imply that our understanding of nature via the standard model would be profoundly shaken if the top quark was shown not to exist with its expected properties. The observation of the top quark is therefore of considerable significance.

1.2 Earlier Top Quark Searches

Direct searches for the top quark have been performed at virtually all of the high-energy collider facilities that have operated in the last twenty years[5]. The most model-independent searches have taken place at e^+e^- colliders, where one looks for the production and decay of a pair of massive fermions. Because of the relatively large mass of the top quark, its decay yields events that are quite spherical and are relatively easy to separate from the background of lighter quark production. The most stringent limits have been set by the LEP collaborations, which require that $M_{top} > 46$ GeV/c^2 at 95% confidence level (CL). These limits are insensitive to the decay modes of the top quark and the coupling of the top quark to the electroweak bosons.

Another relatively model-independent limit is set by measurements of the width of the W boson. Direct and indirect measurements of Γ_W[6] indicate that the top quark is massive enough that the decay channel $W \rightarrow t\bar{b}$ does not contribute to Γ_W. The limit set is $M_{top} > 62$ GeV/c^2 at 95% CL.

Direct searches for the top quark at hadron colliders have focused on two specific models for top quark decay: i) the minimal supersymmetric model (MSSM) where the decay mode $t \rightarrow H^+b$ is also allowed, and ii) the standard model where the top quark decays directly to $t \rightarrow Wb$. The most stringent limit set assuming the MSSM requires that $M_{top} > 96$ GeV/c^2 at 95% CL for the case where $t \rightarrow H^+b$ always and $BR(H^+ \rightarrow \tau\nu_\tau) = 1.0$ [7]. This limit, however, depends on the overall width of the decay $t \rightarrow H^+b$, the Higgs branching fractions (H^+ is expected to preferentially decay to $c\bar{s}$ and $\tau\nu_\tau$ final states) and the H^+ detection efficiency. The DØ collaboration has published the most sensitive standard model search using a 15 pb^{-1} dataset, and has excluded a top quark with mass less than 131 GeV/c^2 at 95% CL [8].

On the other hand, the CDF collaboration published a study of $\sim$ 20 pb^{-1} of data in April 1994 that claimed evidence for top quark production [9]. A total of 12 events were observed in several decay modes above a predicted background of approximately 6 events. The probability that the observed event rate was consistent with a background fluctuation was estimated to be 0.25%. In addition, evidence was presented that the events in the sample were consistent with arising from the production and decay of a $t\bar{t}$ system, and inconsistent with the properties expected of the dominant backgrounds. Although compelling, this observation was statistically limited and the possibility that it arose from a background fluctuation could not be ruled out.

In this report, I will focus on the first results to come from the DØ and CDF top quark searches using data collected in 1994 and early 1995. Both collaborations have acquired over three times more data in the last year, and have now reported conclusive evidence for top quark production [10]. I will describe the analyses performed by both collaborations and compare the two results. I believe an extremely persuasive case has been made that the top quark has been found.

2 Production and Decay of Heavy Top

The production of heavy quarks in 1.8 TeV $p\bar{p}$ collisions is predicted to take place through the two leading-order quantum-chromodynamic (QCD) diagrams

$$q\bar{q} \rightarrow Q\bar{Q} \quad (2)$$

$$gg \rightarrow Q\bar{Q}, \quad (3)$$

with the relative rate of these two processes dictated largely by the mass of the heavy quark (Q), parton distribution functions of the proton and phase space. Top quark pair-production is expected to dominate the production rate; the production of single top quarks through the creation of a virtual W is much smaller and expected to oocur in a relatively small part of phase space (all heavy top quark searches have therefore ignored single top production). The next-to-leading order corrections to processes (2) and (3) are relatively small for heavy quark masses greater than of order 50 GeV/c^2 [11]. More recently, these estimates have been revised taking into account the effects of internal soft-gluon emission [12].

These cross sections are shown in Fig. 1 plotted as a function of the heavy quark mass. The uncertainty in these estimates reflects the theoretical uncertainty in this calculation, which is believed to be the choice of renormalisation scale. For top quark masses above 100 GeV/c^2, the primary contribution to the cross section comes from quark annihilation. This reduces the uncertainties arising from our lack of knowledge of the parton distribution functions of the proton, as these have been accurately measured at large Feynman x, the kinematic region that would dominate very heavy quark production.

Top quark pair production will generate a top quark and anti-top quark that are recoiling against each other in the lab. The production diagrams favour configurations where both top quarks are produced isotropically in the lab frame. The relative motion of the $t\bar{t}$ system is expected to be small in comparison to the transverse momentum[1] (P_T) distribution of the top quark itself [13]. The expected P_T distribution for a heavy top quark has a peak around half the top quark mass with a

[1] I will employ a coordinate system where the proton beam direction defines the $\hat{z}$ axis, and transverse variables such as transverse momentum (P_T) and transverse energy (E_T) are defined relative to this axis. The angle ϕ represents the azimuthal angle about the beam axis and the angle θ represents the polar angle relative to the beam axis. Pseudorapidity $\eta \equiv -\ln\tan(\theta/2)$ will often be employed instead of θ.

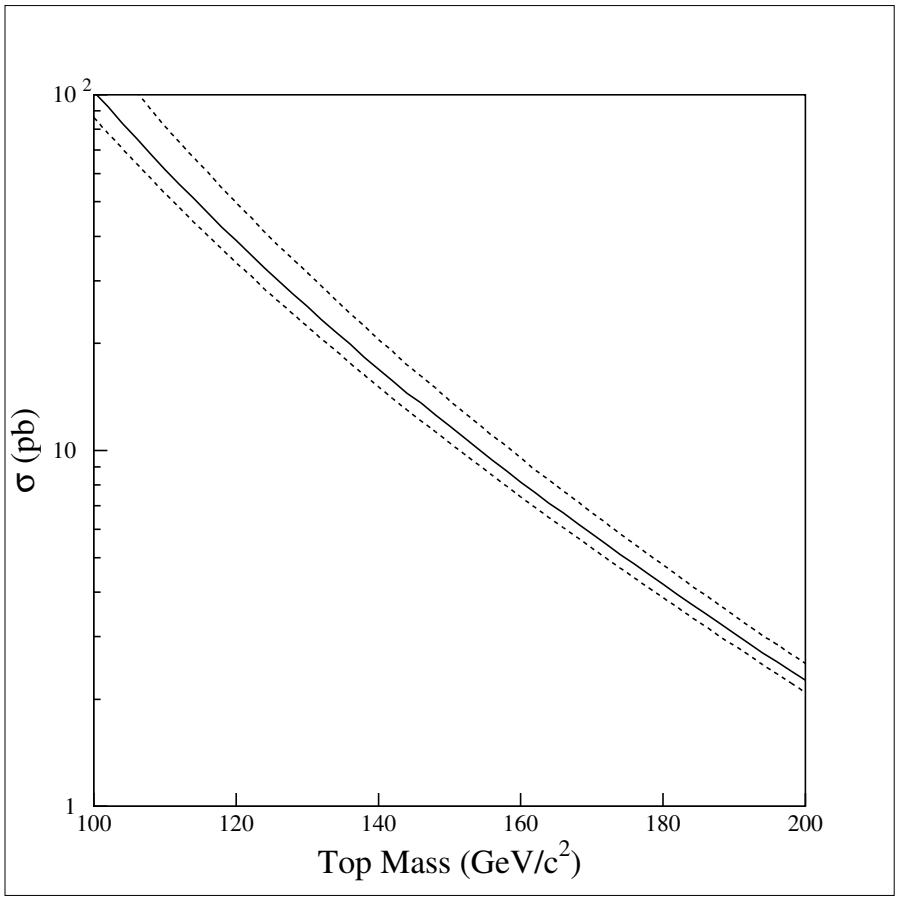

Figure 1: The total cross section for top quark production in 1.8 TeV $p\bar{p}$ collisions. The upper and lower curves are a measure of the theoretical uncertainties in the calculation.

relatively long tail. The pseudorapidity distribution for top quarks is peaked at 0 and falls off rapidly so that most of the top quarks are produced in the "central" region with pseudorapidity $|\eta| < 2$. The combination of a relatively energetic heavy quark produced centrally is ideal from an experimental point of view. The top quark decay products are rather stiff and central, aiding their detection.

The standard model predicts that the top quark will decay almost always via $t \to W^+b$. The W decays approximately 2/3 of the time into $q\bar{q}'$ pairs ($u\bar{d}$ or $c\bar{s}$) and 1/3 of the time into one of the three lepton generations. This results in a decay topology consisting of 6 energetic partons that could either be charged or neutral leptons, or quark jets.

The decay channels involving τ leptons are problematic given the difficulty of cleanly identifying these weakly decaying leptons in a hadron collider environment. They have therefore not been explicitly included in the searches I describe below. The final states involving 6 quark jets suffer an enormous background from QCD multijet production, with estimates of intrinsic signal-to-noise of $< 10^{-4}$. Because of these large backgrounds, this channel has not been the focus of most of the effort, and I will ignore it here also.

With these considerations, there are five final states that are experimentally accessible:

$$\begin{aligned}
t\,\overline{t} &\rightarrow e^{+}\nu_{e}b\; e^{-}\bar{\nu}_{e}\bar{b} \quad (1/81) \\
t\,\overline{t} &\rightarrow \mu^{+}\nu_{\mu}b\; \mu^{-}\bar{\nu}_{\mu}\bar{b} \quad (1/81) \\
t\,\overline{t} &\rightarrow e^{\pm}\nu_{e}b\; \mu^{\mp}\nu_{\mu}\bar{b} \quad (2/81) \\
t\,\overline{t} &\rightarrow e^{\pm}\nu_{e}b\; q\bar{q}'\bar{b} \quad (12/81) \\
t\,\overline{t} &\rightarrow \mu^{\pm}\nu_{\mu}b\; q\bar{q}'\bar{b} \quad (12/81),
\end{aligned} \tag{4}$$

where I have also listed the expected standard model branching ratios for each channel. The first three dilepton channels turn out to be the cleanest final states, as the requirement of two energetic charged leptons and neutrinos virtually eliminate all backgrounds. They suffer from rather small branching fractions and are therefore the most statistically limited. The last two lepton + jets final states together correspond to approximately 30% of the $t\,\overline{t}$ branching fraction. However, these channels face the largest potential backgrounds.

3 Backgrounds to a Standard Model Top Quark Search

Top quark production is an extremely rare process in $\overline{p}\,p$ collisions; its cross section of less than 100 pb can be compared with the total $\overline{p}\,p$ cross section of over 50 mb (almost nine orders of magnitude difference). Since the total cross section is dominated by "soft" QCD interactions, the top quark cross section can be more fairly compared with the cross section for other high Q^2 production processes, such as inclusive W production (20 nb), Z production (2 nb) and WW and WZ production (10 and 5 pb, respectively). These higher Q^2 processes are the sources of the most severe background to $t\,\overline{t}$ production.

It is necessary to control these backgrounds so that one can be sensitive to a top quark signal. All the channels listed in (4) involve an energetic charged electron or muon, and one or more energetic neutrinos. The requirement of these two signatures in the final state using the DØ and CDF lepton identification systems are sufficient to adequately control the backgrounds associated with jets that might satisfy the lepton ID criteria. The remaining backgrounds are dominated by physics processes that generate real leptons in the final state.

In the case of the dielectron and dimuon modes, the single largest background comes from Drell-Yan production (including $Z \rightarrow e^{+}e^{-}$ and $Z \rightarrow \mu^{+}\mu^{-}$). This is controlled by requiring a neutrino signature as well as additional jet activity. The single largest physics background in the $e^{\pm}\mu^{\mp}$ final state comes from $Z \rightarrow \tau^{+}\tau^{-}$ decay, which can be similarily reduced by the requirement of a neutrino signature and additional jets.

The single largest physics background to lepton+jets final states come from inclusive W production where additional jets are produced via initial and final state

Jet Multiplicity	σB (pb)	$\sigma_T B$ (pb)
0	$1740 \pm 31 \pm 288$	$1753 \pm 26 \pm 123$
1	$336 \pm 14 \pm 63$	$287 \pm 4 \pm 21$
2	$76 \pm 12 \pm 18$	$59 \pm 2 \pm 5$
3	$14 \pm 3 \pm 3$	$11.0 \pm 0.3 \pm 1.0$
4	$4.0 \pm 1.6 \pm 1.2$	$2.0 \pm 0.1 \pm 0.3$

Table 1: The W+jet production cross section times the branching ratio for $W \rightarrow l^+\nu_l$ as a function of jet multiplicity. The second column presents the observed cross sections for jets with corrected transverse energy > 15 GeV and $|\eta| < 2.4$. The third column shows the predicted QCD cross section based on a VECBOS Monte Carlo calculation.

radiation [14]. The intrinsic rate for this background depends strongly on the multiplicity requirements placed on the jet candidates, as shown in Table 1 where the observed W+jets production cross section is presented as a function of jet multiplicity and compared with a QCD Monte Carlo prediction [15]. One can see from these rates that this background can overwhelm a $t\,\overline{t}$ signal. More stringent kinematic cuts can be applied to reject the W+jets events, taking advantage of the fact that the $t\,\overline{t}$ final states, on average, generate higher E_T W bosons and additional jets. Alternatively, since the $t\,\overline{t}$ final state has two b quark jets in it, the requirement that one or more jets are consistent with arising from the fragmentation of a b quark will preferentially reduce the W+jets background. Both of these techniques have been employed.

4 The Tevatron Collider

The Tevatron Collider is a 6 km circumference proton-antiproton storage ring that creates $\overline{p}\,p$ collisions at a centre-of-mass energy of 1.8 TeV. In its current configuration, the collider operates with six bunches of protons and six bunches of counter-rotating antiprotons that are brought into collision at two intersection points in the ring named B0 and D0. The B0 and D0 interaction regions house the CDF and D$\emptyset$ detectors.

The Tevatron embarked on a multi-year collider run starting in December 1992. The first stage of the run, known as Run IA, continued through till August 1993, at which time approximately 30 pb^{-1} had been delivered to each interaction region. The second stage of the run commenced in August 1994 and will continue till the end of 1995. By February 1995, the collider had delivered an additional 80 pb^{-1} to each interaction region. The maximum luminosity of the Collider during this period has been 1.7×10^{31} cm^{-2}s^{-1}, and has been consistently increasing.

Run IB run is scheduled to end in February 1996, with a total of $\sim$ 150 pb^{-1} delivered to each interaction region.

5 The DØ and CDF Experiments

The DØ and CDF detectors have been designed to trigger and record the high P_T collisions that result when two partons in the $\overline{p}\,p$ system undergo a hard scatter. Both instruments detect electrons, muons, neutrinos and quark and gluon jets using a set of complementary subdetectors. However, they accomplish this common goal in rather different ways.

5.1 The DØ Detector

The DØ detector was designed with the philosophy that a uniform, hermetic, highly-segmented calorimeter should form the core of the detector [16]. A cut-away view of the detector is shown in Fig. 2. The DØ calorimeter employs a Uranium absorber up to nine interaction lengths thick and a liquid Argon readout system. This provides excellent hermeticity and uniformity, except perhaps in the transition region between the barrel and endcap cryostats. The overall resolution of the DØ calorimeter is

$$\frac{\sigma_E}{E} = \frac{0.15}{\sqrt{E}} \oplus 0.004 \text{ for electromagnetic showers} \tag{5}$$

$$\frac{\sigma_E}{E} = \frac{0.80}{\sqrt{E}} \text{ for hadrons.} \tag{6}$$

A muon system consisting of charged particle detectors and 1.9 Tesla toroidal magnets located outside the calorimeter provides good muon identification. The DØ detector identifies muon candidates in the region $|\eta| < 3.3$ using a set of muon tracking chambers consisting of proportional drift tubes outside the calorimeter. The chambers are located interior and exterior to the large toroidal magnetic field. The deflection of the muon candidates in the magnetic field provides a momentum measurement with an accuracy of

$$\sigma\left(\frac{1}{p}\right) = \frac{0.18\,(p-2)}{p^2} \oplus 0.008, \tag{7}$$

where p is the muon momentum measured in GeV/c.

A vertex, central and forward drift chambers provide charged particle detection in the interval $|\eta| < 3.2$. The tracking system does not incorporate a magnetic field, as the presence of a magnetic coil would degrade calorimeter performance.

5.2 The CDF Detector

The CDF detector [17] consists of a high-precision tracking system in a 1.4 T solenoid magnetic field, surrounded by a hermetic highly-segemented calorimeter, as shown in Fig. 3. The tracking system consists of three independent devices arranged coaxial to the beam line. A 4-layer silicon-strip detector (SVX) with inner and outer radii of 3.0 and 7.9 cm provides of order 40 μ precision on the impact parameter of

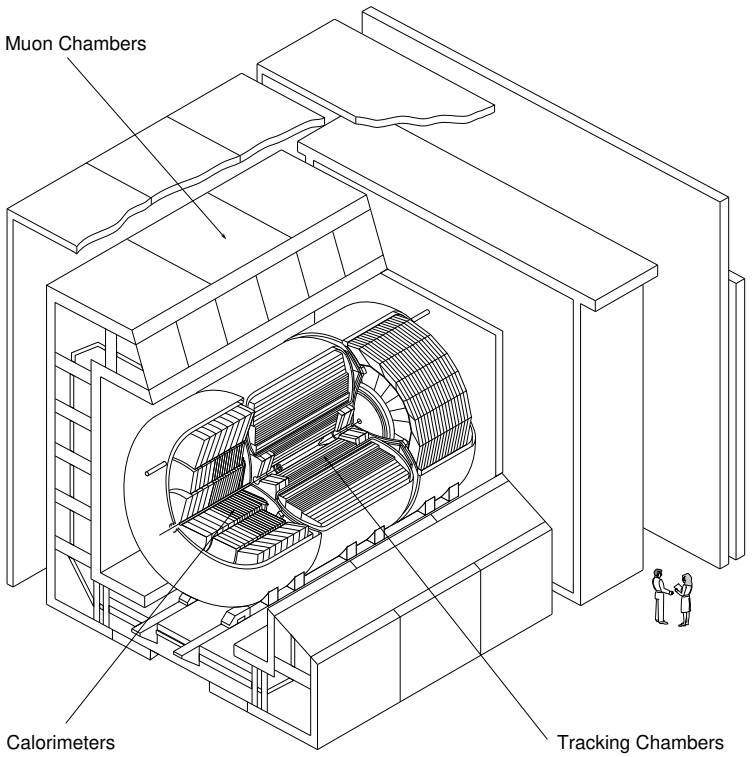

Figure 2: A cut-away view of the DØ detector. The inner tracking detectors are surrounded by the calorimeter cryostats, and both are situated inside the toroidal magnet. Planes of chambers outside the magnet provide for muon identification and momentum measurement.

individual charged track trajectories extrapolated to the beam line. A set of time projection chambers (VTX) instrument the tracking region between 12 and 22 cm in radius, providing high-precision tracking in the $r-z$ plane. An 84-layer drift chamber (CTC) detects charged particles in the region between 30 and 132 cm from the beamline. Together, these detectors measure particle momentum to a precision σ_p given by

$$\frac{\sigma_{p_T}}{p_T} = 0.0009 p_T \oplus 0.0066, \tag{8}$$

for particles with $p_T \gtrsim 0.35$ GeV/c. The central calorimeter instruments the region $|\eta| < 1.1$, and is comprised of projective towers of size $\Delta\eta \times \Delta\phi = 0.1 \times 0.26$ radians. Each tower is made of a sandwich of Pb or Fe plates interleaved with scintillator. A Pb sandwich 25 radiation lengths thick is used to measure electromagnetic shower energies. An iron-scintillator sandwich approximately 5 interaction lengths thick is used to detect hadronic showers. Plug and Forward calorimeters instrument the region $1.1 < |\eta| < 4.2$, and consist of similar absorber material. The showers are detected with proportional wire chambers as they provide for a radiation resistant detector

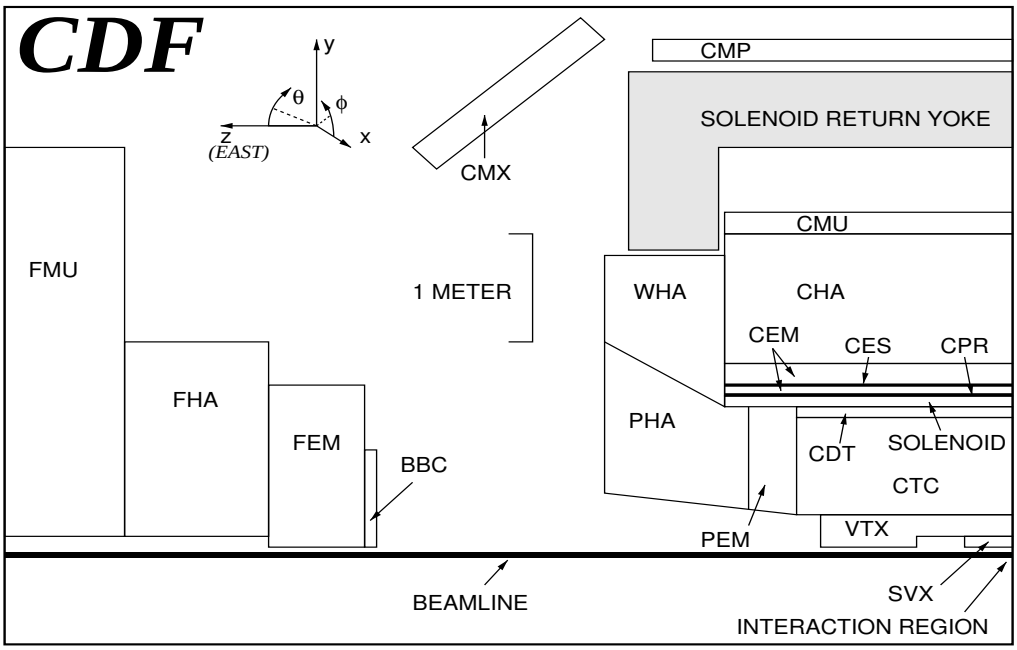

Figure 3: A schematic view of one quarter of the CDF detector. The interaction point is at the lower right corner of the figure.

system. The presence of solenoid magnet and a significant amount of material in front of the calorimeter leads to some compromise in calorimeter performance. The overall resolution of the CDF calorimeter is

$$\frac{\sigma_E}{E} = \frac{0.137}{\sqrt{E}} \oplus 0.02 \quad \text{(for electromagnetic showers)} \tag{9}$$

$$\frac{\sigma_E}{E} = \frac{0.50}{\sqrt{E}} \oplus 0.03 \quad \text{(for hadrons)}. \tag{10}$$

Planar drift chambers located outside the calorimeter volume detect muons penetrating the calorimeter absorber, but precise muon momentum and direction come from the associated charged track detected in the inner tracking system. The central muon system is able to detect muons within the pseudorapidity interval $|\eta| < 1.0$. A forward muon system (FMU) consisting of large toriodal magnets surrounded by drift chambers and scintillator counters detect muons in the rapidity region $2.2 \leq |\eta| \leq 3.5$.

5.3 Triggering and Data Acquisition

Pair production of standard model top quarks and their subsequent decay into either the dilepton or lepton+jets mode yields a signature that is relatively straightforward to trigger on. Both detectors employ multi-level trigger systems where at each level more information is brought together to form a decision. The trigger requirement of at least one energetic electron or muon is the primary tool used in identifying online a sample of top quark candidate events that are subsequently studied offline.

The requirement of at least one high P_T electron or muon in both CDF and D$\emptyset$ is imposed efficiently in the trigger. The production of leptons above a transverse energy of 15 GeV is dominated in both experiments by b and c quark production, and by inclusive $W^{\pm}$ boson production. For example, in CDF, the inclusive electron trigger is implemented with the following requirements:

1. The level 1 trigger demands that at least one calorimeter trigger cell with $\Delta\phi \times \Delta\eta = 0.26 \times 0.2$ has > 6 GeV of electromagnetic energy.

2. The level 2 trigger demands that there be a charged track candidate pointing at an electromagnetic energy cluster, and requires that the cluster properties be consistent with those of an electromagnetic shower.

3. The level 3 trigger requires the presence of an electromagnetic cluster associated with a charged track reconstructed using the standard offline algorithms. Further quality cuts on the properties of the electromagnetic shower are also made.

These reduce the overall cross section of candidate events to approximately 50 nb, of which approximately 30% is comprised of real electrons. For comparison, the rate of $W \rightarrow e\nu_e$ in this sample is of order 1 nb. The efficiency of this trigger for isolated electrons with $20 < E_T < 150$ GeV is $92.8 \pm 0.2\%$.

As another example, the D$\emptyset$ detector triggers on a sample of inclusive muon candidates by using a two level decision process:

1. The level 1 trigger demands the presence of a charged track stub in the muon toroidal spectrometer with a $p_T > 3$ GeV/c.

2. The level 2 trigger demands a high quality muon candidate consisting of a muon candidate in the muon system matched to a charged track observed in the central tracking system. The central track candidate must be reconstructed in all 3 dimensions, must be consistent with coming from the event interaction, and must have P_T greater than 5 or 8 GeV/c, depending on the specific muon trigger.

The efficiency of this trigger is estimated to be $67 \pm 3\%$.

Both experiments employ inclusive electron and muon triggers, as well as triggers that identify smaller samples of events useful to the top search. Since the backgrounds to the dilepton sample are relatively small, it is convenient to identify the candidate events immediately in the trigger so that they can be analysed as soon as possible. A high-P_T dilepton trigger requiring at least two electron or muon candidates is therefore employed to flag these candidates immediately. The cross section for this trigger is only a few nb.

At a luminosity of 2×10^{31} cm^{-2}s^{-1}, a trigger cross section of 300 nb corresponds to an event rate of 6 Hz, which can be comfortably recorded and analyzed. Note,

however, that even with a cross section of 10 nb, the total data sample for an integrated luminosity of 50 pb^{-1} will consist of 500 000 events, with each event comprised of order 200 kbytes of information.

5.4 The Run IA and IB Datasets

The Tevatron Collider started up after a three year shut-down in fall 1992, and continued running through the summer of 1993. As this was the D$\emptyset$ detector's first collider run, it was remarkable that the collaboration was able to successfully use 40-50% of the collisions for their physics studies. The CDF collaboration gathered 19.6 ± 0.7 pb^{-1} of data during this period.

From the start of Run 1B in 1994 to February 1995, the Tevatron Collider had delivered over 100 pb^{-1} of collisions to each detector. The D$\emptyset$ and CDF collaborations had recorded and analysed $\sim$ 45 pb^{-1} of this data by this date, giving the the two collaborations total Run 1 datasets of 50 and 67 pb^{-1}, respectively.

In between Run 1A and 1B, both collaborations made incremental improvements to their detectors. The D$\emptyset$ detector's muon trigger was improved and various detector subsystems were modified with the goal of improving overall robustness and efficiency. The CDF collaboration replaced the original 4-layer SVX detector with a mechanically identical device that used newer, radiation-hard silicon strip wafers, and employed an AC-coupled readout design. The new detector, known as the SVX', has much better signal-to-noise and is fundamentally better understood.

5.5 Event Reconstruction

Given the large number of partons that arise from the decay of the $t\bar{t}$ system, each detector is required to reconstruct with good efficiency high energy electrons and muons, the jets resulting from the fragmentation of high energy quarks, and the presence of one or more neutrinos by the imbalance of total transverse energy in the collision.

High energy electrons and muons are identified in both detectors by the charged track left in the central tracking systems, and by the behaviour of the leptons in the calorimeters and muon identification systems outside the calorimeters. Electrons will generate an electromagnetic shower in the calorimeter, with a lateral and longitudinal shower profile quite distinct from the shower intitiated by a charged hadron. Muons are readily identified as they generally pass unimpeded through the calorimeter and are detected outside the calorimeters as charged particles that point back to the particle trajectory in the central tracker. The CDF electron and muon reconstruction algorithms have efficiencies of $84 \pm 2\%$ and $90.6 \pm 1.4\%$ for leptons from W boson decays. The D$\emptyset$ electron reconstruction has an efficiency of $72 \pm 3\%$. These efficiencies are quoted for electron and muon candidates that have already passed the trigger requirements discussed earlier.

Neutrinos can only be detected by requiring that they have sufficient transverse energy that the total measured energy flow sum to a value inconsistent with zero. In

practical terms, this energy flow vector is known as missing transverse energy ($\not\!\!E_T$). Note that we cannot use the imbalance in energy flow along the beamline in this case as one can expect a significant imbalance due to the differing momentum of the partons in the proton and antiproton that collide to produce the $t\bar{t}$ system. The resolution in $\not\!\!E_T$ is driven by both the uniformity of the calorimeter and its inherent energy resolution. D$\emptyset$ has a missing transverse energy resolution in each transverse coordinate of

$$\sigma_x = 1.08 + 0.019 \left(\sum E_T \right) \text{ GeV}, \tag{11}$$

where the summation gives the total scalar transverse energy observed in the calorimeter. CDF's transverse energy resolution is approximately 15-20% worse, which has a modest impact on its neutrino detection ability.

Jets are constructed in both detectors as clusters of transverse energy within a fixed cone defined in $\eta - \phi$ space [18]. The size of this cone is determined by the competing requirements of making it large enough to capture most of the energy associated with the fragmentation of a quark or gluon, and yet small enough that it doesn't include energy associated with nearby high energy partons or from the "underlying" event. The latter effect in itself contributes on average approximately 2 GeV per unit in $\eta - \phi$ space, but fluctuations in the underlying event affect the jet energy resolution (the size of this effect depends on the rate of multiple interactions). Monte Carlo (MC) calculations using a variety of models for quark fragmentation and underlying event assumptions, as well as studies of the underlying events have indicated that a jet cluster cone size substantially smaller than the traditional $\eta - \phi$ radii of 0.7 or 1.0 employed in QCD studies is required. The CDF analysis employs a cone cluster size of 0.4 in its top quark search, whereas the D$\emptyset$ collaboration has chosen to work with a cone size of 0.5.

The reconstruction of the final state partons and the requirement that most if not all daughters are reconstructed is not sufficient to reject all backgrounds to $t\bar{t}$ production. There are other kinematical variables that discriminate between $t\bar{t}$ and background events, most of them taking advantage of the fact that heavy top quark production will generate final state daughters that are on average quite energetic. This motivates the use of a variable called H_T defined as

$$H_T = \sum_{i=1}^{N_p} E_T^i, \tag{12}$$

where the sum is over all the jets and the leading electron cluster (in those channels where at least one electron is required). This variable is used by the D$\emptyset$ collaboration in both their dilepton and lepton+jets analysis, and its effectiveness in improving the signal-to-noise in the dilepton and lepton + jets channels is illustrated in Fig. 4. The CDF collaboration has recently reported the results of a top analysis using a similar variable [19].

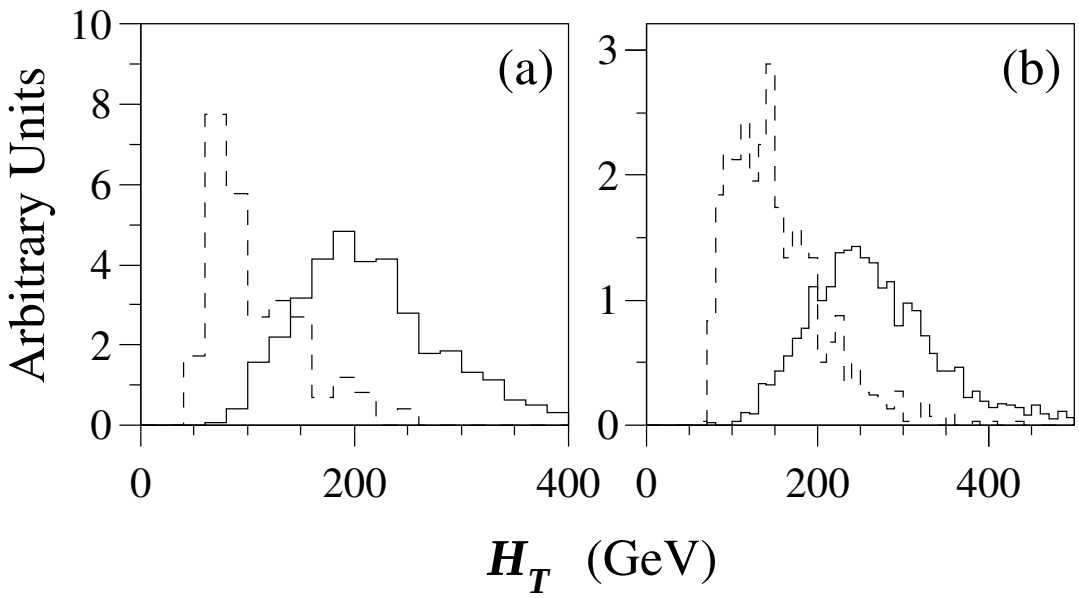

Figure 4: The H_T distributions for $e\mu$+ jet events (a) and lepton + jet events (b). The solid histograms are the distributions expected from $t\bar{t}$ events for a top quark mass of 200 GeV/c^2. The dashed histograms are the expected distributions for the dominant backgrounds to $t\bar{t}$ production in both channels.

An additional kinematic variable known as aplanarity ($\mathcal{A}$) [20] has been employed by the D$\emptyset$ collaboration. This, as its name suggests, is a measure of how spherical a candidate event is: $t\bar{t}$ events are expected to have larger values of $\mathcal{A}$ than the corresponding physical backgrounds.

The final tool used in the reconstruction of $t\bar{t}$ events is the identification or "tagging" of jets that arise from the b quarks. There are two techniques employed by the collaborations. The first takes advantage of the fact that bottom hadrons decay semi-leptonically into electrons or muons about 20% of the time. D$\emptyset$ and CDF therefore search the interior of each jet cone for a muon candidate. CDF also searches for low-energy electron candidates that can be associated with a jet cluster. Because there are two b quarks in each $t\bar{t}$ decay, the efficiency of this soft lepton (SLT) tagging scheme ranges from 10-15%. The second technique is used exclusively by CDF and takes advantage of the long-lived nature of bottom hadrons and the SVX (or SVX') detector. A seach is performed for several charged tracks detected in the SVX that form a secondary vertex a significant distance from the primary interaction. The efficiency of this tagging scheme depends crucially on the performance of the SVX/SVX'. It is estimated that over 40% of all $t\bar{t}$ decays will have the presence of at least one SVX tag.

6 The Dilepton Top Quark Search

6.1 Dilepton Data Selection

The dilepton decay modes are the cleanest channel in which one would expect to observe a heavy top quark. They suffer from the relatively small total branching fraction of $t\bar{t}$ into these modes (a total of 4%), and from the presence of two neutrinos in the final state that are not individually observable.

The dilepton searches break down into three separate channels, the e^+e^-, $\mu^+\mu^-$ and $e^\pm\mu^\mp$ final states. The CDF analysis requires two isolated lepton candidates, each with $P_T > 20$ GeV/c and with $|\eta| < 1.0$. The candidates must satisfy standard lepton quality requirements that ensure high efficiency and high rejection from energetic, isolated charged hadrons. There are 2079 ee candidates, 2148 $\mu\mu$ candidates and 25 $e\mu$ candidates after these kinematical cuts. The large ee and $\mu\mu$ candidate samples are the result of Z° and Drell-Yan production, as can be seen by examining the invariant mass (M_{ll}) distribution of the dilepton system. This background is removed by rejecting those events with

$$75 < M_{ll} < 105 \text{ GeV/c}^2. \tag{13}$$

This leaves 215, 233 and 25 candidate events in the ee, $\mu\mu$ and $e\mu$ channels, respectively.

In addition, the events are required to have $\not\!\!E_T > 25$ GeV and at least two jet clusters with $E_T > 10$ GeV and $|\eta| < 2.0$, since $t\bar{t}$ events are expected to have two energetic neutrinos and a b quark and anti-quark in the final state. This still leaves a background in the ee and $\mu\mu$ sample from Drell-Yan production where the $\not\!\!E_T$ signal arises from an accompanying jet that is mismeasured. The distribution of the opening angle between the missing transverse energy vector and the closest jet or charged lepton candidate in the event versus the missing transverse energy for each jet multiplicity is shown in Figs. 5 and 6 for the $\mu\mu$ and $e\mu$ channels, respectively. There is a clear cluster of events at small $\not\!\!E_T$-jet opening angles that extend to higher $\not\!\!E_T$ in the $\mu\mu$ (and ee) samples. The same enhancement is not present in the $e\mu$ sample, which has no Drell-Yan contamination. A stiffer $\not\!\!E_T$ cut requiring at least 50 GeV of missing transverse energy is imposed on those events that have $\not\!\!E_T$-jet opening angles less than 20°. The same region is occupied preferentially by backgrounds from $Z \to \tau^+\tau^-$ in the $e\mu$ sample so it is also removed.

This leaves a total of 7 candidate CDF events, 5 in the $e\mu$ channel and two in the $\mu\mu$ channel. No dielectron events survive the selection. One of the $\mu\mu$ events has an energetic photon candidate with a $\mu^+\mu^-\gamma$ invariant mass consistent with that of a Z°. Although the expected background from radiative $Z_\circ$ decay is only 0.04 events, the $\mu^+\mu^-\gamma$ candidate is removed from the sample in order to be conservative.

The DØ analysis requires two high P_T leptons; both leptons are required to have $P_T > 20$ GeV/c in the ee channel, $P_T > 15$ GeV/c in the $\mu\mu$ channel, and $P_T > 15(12)$ GeV/c for the electron (muon) in the $e\mu$ channel. A $\not\!\!E_T$ cut requiring at least 20 GeV

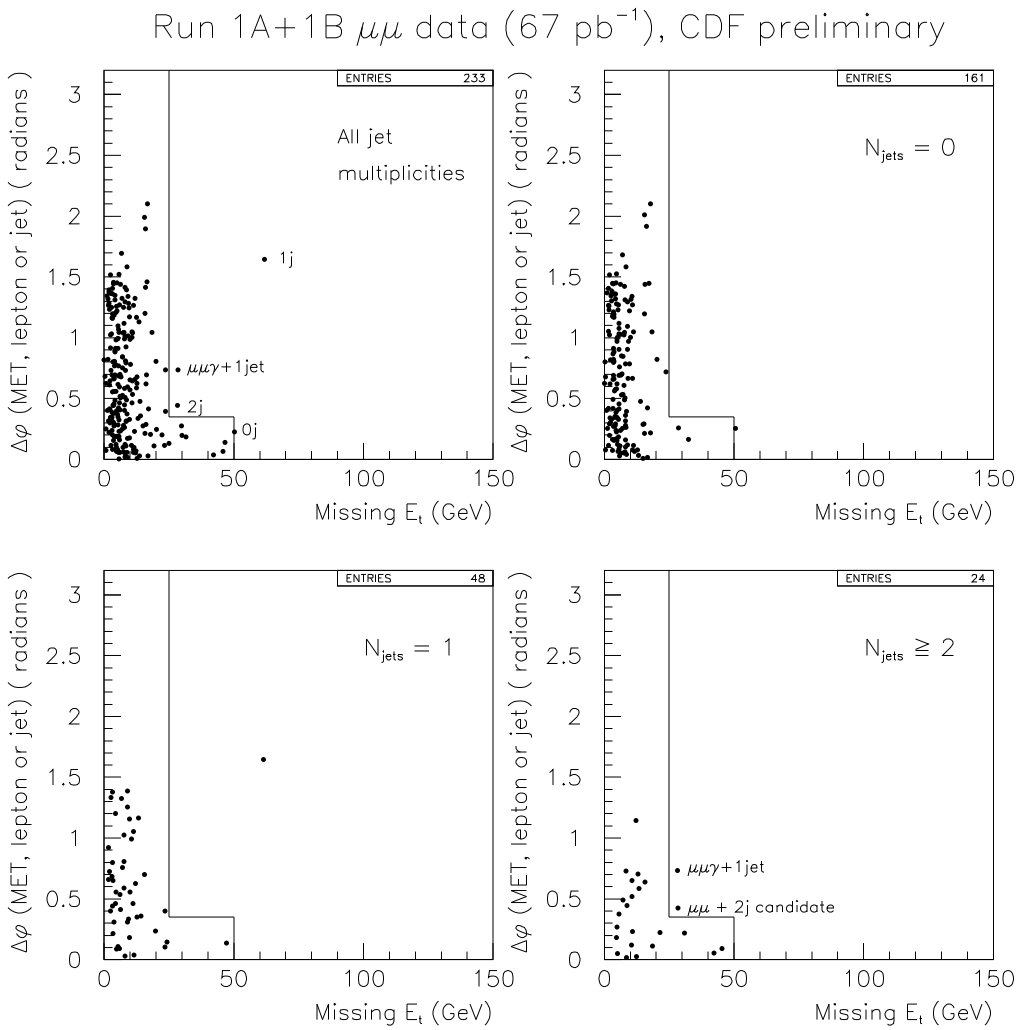

Figure 5: The distribution of the azimuthal opening angle between the missing E_T vector and the highest energy jet or lepton versus the events $\not\!\!E_T$ is shown for all events, and for events with 0, 1 and ≥ 2 jets in the $\mu\mu$ channel. The boundary shows the cuts placed to reject the remaining Drell-Yan background.

and 25 GeV is placed on the $e\mu$ and ee channels, respectively (no $\not\!\!E_T$ requirement is placed on $\mu\mu$ candidate events). The selection requires at least two jets with corrected transverse energy > 15 with $|\eta| < 2.5$. Finally, ee and $e\mu$ candidate events are required to have $H_T > 120$ GeV and $\mu\mu$ events are required to have $H_T > 100$ GeV.

This leaves a total of 3 dilepton candidate events in the D$\emptyset$ dataset. There are 2 $e\mu$ events, no ee events, and 1 $\mu\mu$ event. The integrated luminosities corresponding to these three channels is 47.9 ± 5.7, 55.7 ± 6.7 and 44.2 ± 5.3 pb^{-1}, respectively. The expected number of observed events arising from $t\,\overline{t}$ production is shown in Table 2.

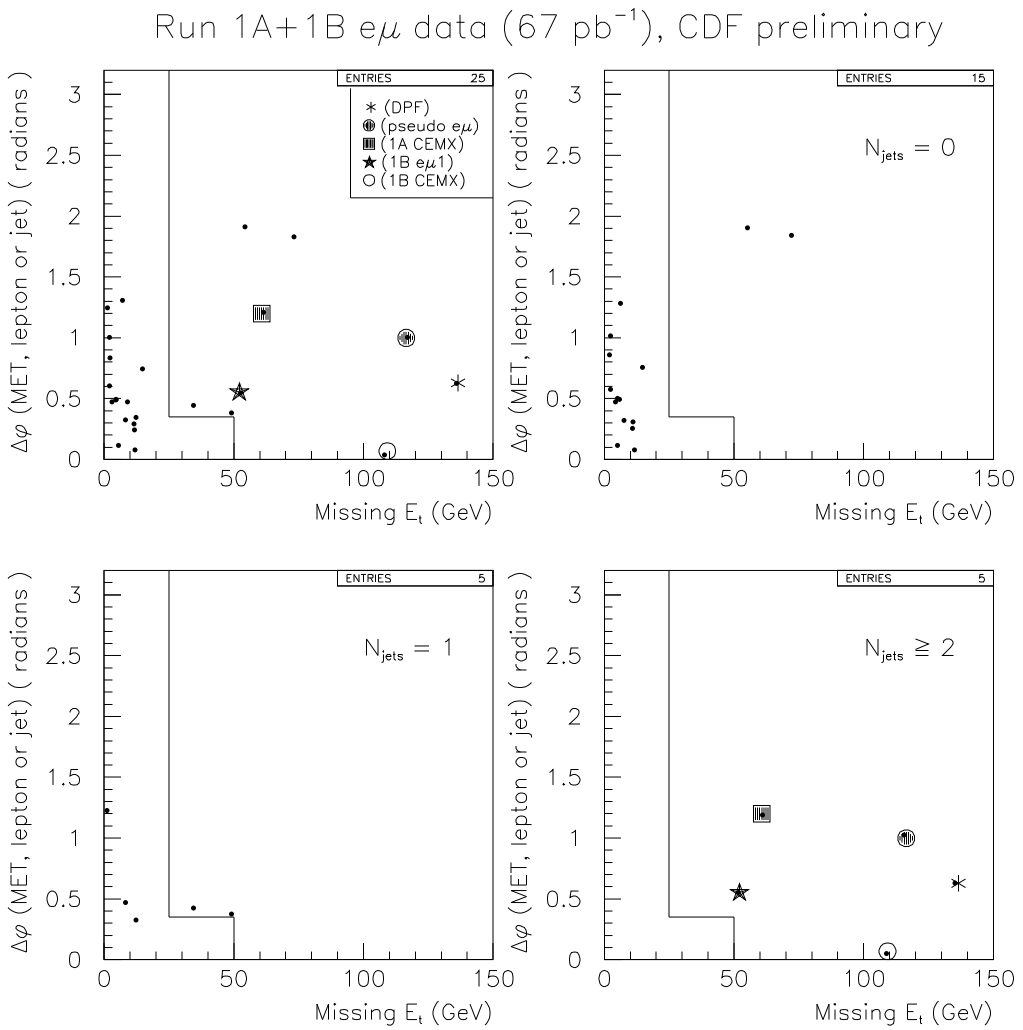

Figure 6: The distribution of the azimuthal opening angle between the missing E_T vector and the highest energy jet or lepton versus the events $\not\!\!E_T$ is shown for all events, and then for events with 0, 1 and ≥ 2 jets in the $e\mu$ channel. The boundary shows the cuts placed to reject the $Z \rightarrow \tau^+\tau^-$ background.

6.2 Dilepton Backgrounds

The number of dilepton events observed by CDF and D$\emptyset$ is consistent with the rate expected from $t\bar{t}$ production for a top quark mass of order 140 to 150 GeV/c^2. It is necessary to accurately estimate the number of events expected from standard model background processes in order to interpret these event rates.

The most serious potential background comes from Z° production, followed by the decay $Z^\circ \rightarrow \tau^+\tau^-$. The τ leptons then decay leptonically leaving the dilepton signature and missing energy from the four neutrinos. The rate of this background surviving the selection criteria can be accurately estimated using the observed Z° kinematics in the dielectron and dimuon channels and simulating the decay of the tau leptons. Other standard model sources of dileptons are divector boson produc-

Mass (GeV/c^2)	D$\emptyset$	CDF
150	2.4	6.2
160	2.0	4.4
170	1.6	3.0
180	1.2	2.4

Table 2: The expected number of dilepton events arising from $t\bar{t}$ production for the D$\emptyset$ and CDF selections as a function of top quark mass. The uncertainties on these yields are of order 25-30%. The central value for the theoretical prediction for the $t\bar{t}$ cross section is assumed.

Background	CDF	D$\emptyset$
$Z \to \tau^+\tau^-$	0.38 ± 0.07	0.16 ± 0.09
Drell Yan	0.44 ± 0.28	0.26 ± 0.06
Fake $e^{\pm}$ or $\mu^{\pm}$	0.23 ± 0.15	0.16 ± 0.08
$W^+W^-/W^{\pm}Z^{\circ}$	0.38 ± 0.07	0.04 ± 0.03
Heavy quarks	0.03 ± 0.02	0.03 ± 0.03
Total	1.3 ± 0.3	0.65 ± 0.15

Table 3: The predicted number of background events expected to survive the CDF and D$\emptyset$ dilepton analyses. Only the WW and heavy quark rates are estimated based on Monte Carlo calculations in the CDF analysis.

tion, $b\bar{b}$ and $c\bar{c}$ production, and Drell-Yan production. Most of these are either very small (e.g., the backgrounds from WW and WZ production) or can be estimated reliably from collider data (e.g. heavy quark production). Jets misidentified as leptons are a background source that can be accurately estimated. CDF uses the strong correlation between fake lepton candidates and the larger energy flow in proximity to the candidate. D$\emptyset$ employs similar techniques to estimate this background.

The estimated background rates in the three channels are listed in Table 3 and total to 1.3 ± 0.3 and 0.65 ± 0.15 for the CDF and D$\emptyset$ analyses, respectively. In both cases, there is an excess of observed candidate events above the expected backgrounds.

The significance of this observation can be quantified in a number of ways. One method is to ask how likely this observation is in the absence of $t\bar{t}$ production (the null hypothesis). The answer to this is an exercise in classical statistics [21], where one convolutes the Poisson distribution of expected background events with the uncertainty in this expected rate. The significance of the CDF observation is then 3×10^{-3}; the significance of the D$\emptyset$ observation is 3×10^{-2}.

In themselves, each observation cannot rule out the possibility that the observed events may be due to background sources. Taken together, they make the background-

only hypothesis very unlikely.[2] The obvious next step is to seek independent confirmation.

6.3 B Tagging in the Dilepton Sample

If the dilepton sample has a contribution from $t\bar{t}$ production, it is reasonable to search for evidence that two b quarks are being produced in association with the dilepton pair and neutrinos.

The CDF collaboration has examined these events for such indications using the b tagging algorithms described in detail in the following section. Three of the six events have a total of five tagged jets, three with SLT tags and two with SVX tags. CDF estimates that only 0.5 events would be expected from non-$t\bar{t}$ standard model sources, whereas one would expect 3.6 tags if the events arose from the expected mixture of background and $t\bar{t}$ production. The data is certainly consistent with the $t\bar{t}$ hypothesis, further motivating a detailed study of the lepton+jets data.

7 The Lepton+Jets Top Quark Search

Both collaborations begin their lepton+jets analysis from a data sample dominated by inclusive $W^{\pm}$ production. They require events with significant $\not\!\!E_T$ and a well-identified, high transverse momentum electron or muon. DØ requires the presence of an isolated electron with $E_T > 20$ GeV, and $\not\!\!E_T > 25$ GeV to identify an inclusive $W^{\pm} \to e\nu_e$ sample and an isolated muon with $p_T > 15$ GeV/c, and $\not\!\!E_T > 20$ GeV to identify a $W^{\pm} \to \mu^{\pm}\nu_{\mu}$ sample. CDF requires $\not\!\!E_T > 20$ GeV and a charged lepton be in the central detector with $P_T > 20$ GeV/c and $|\eta| < 1.0$. The transverse mass distribution for the resulting candidate events,

$$M_T \equiv \sqrt{2E_T \not\!\!E_T(1 - \cos\phi_{l\nu})}, \tag{14}$$

shows a clear Jacobian distribution, as illustrated by the CDF data shown in Fig. 7.

7.1 The DØ Lepton+Jets Search

7.1.1 The DØ Kinematic Analysis

The production of $W^{\pm}$ bosons accompanied by additional jets form the largest single background in the lepton+jets search. However, there are significant differences in the kinematics of the partons in the $t\bar{t}$ and W+jets final state that can be used to differentiate between these processes. For example, the H_T distribution is compared for the $t\bar{t}$ and W+jets final state in Fig. 4(b). One sees that this variable provides

[2] One cannot simply multiply the two significances together. To combine these observations, one could define a single statistic (like the total number of observed events in both experiments) and then model the fluctuations of this variable in the case of the null hypothesis. This would give a larger probability of a background hypothesis than the product of the two probabilities.

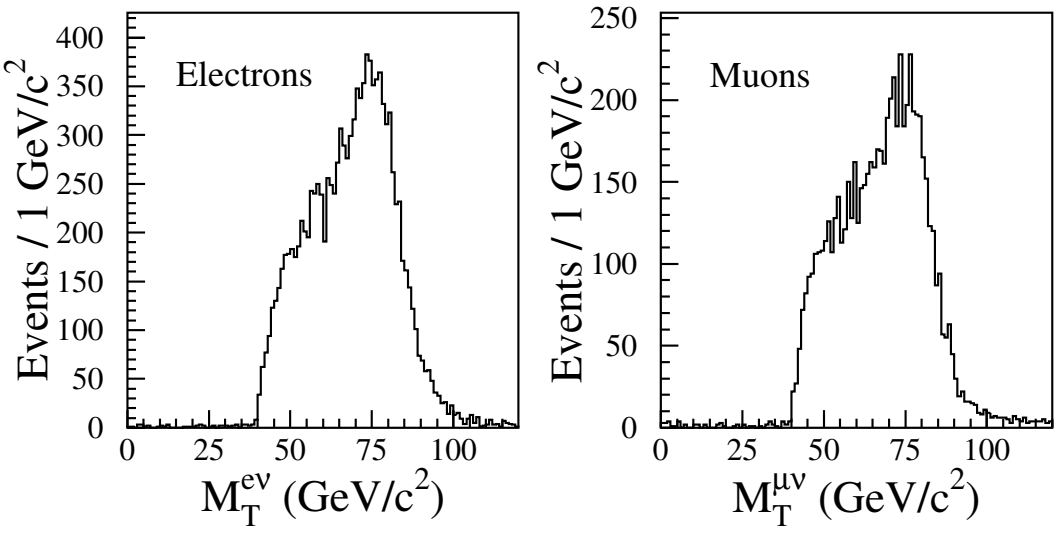

Figure 7: The transverse mass distribution for the CDF electron and muon samples after requiring a well-identified charged lepton and missing transverse energy > 20 GeV. These data are from Run 1A only.

significant separation between signal and background with only a modest loss of signal.

The D$\emptyset$ collaboration defines a $t\bar{t}$ candidate sample by requiring that $H_T > 200$ GeV, that there be at least four jets in the final state with $E_T > 15$ GeV and $|\eta| < 2.0$, and that the aplanarity of the event > 0.05. This leaves 5 $e^{\pm}+$ jet events and 3 $\mu^{\pm}+$ jet events in the sample. They expect to observe 3.8 ± 0.6 events from $t\bar{t}$ production in this sample for a top quark mass of 180 GeV/c^2.

The backgrounds to $t\bar{t}$ production in this sample are dominated by the inclusive $W+$jets process. In order to estimate the size of this background, one can use the rate of observed events in the $W+1$, $W+2$, and $W+3$ jet sample and extrapolate that to the number of events in the $W+ \geq 4$ jet sample. It is expected that the ratio of $W+n$ jet events to $W+(n-1)$ jet events will be constant given the same jet requirements[14] when the H_T and aplanarity cuts are removed. This prediction can be tested using the $W+1$ jets, $W+2$ and $W+3$ jet samples where one expects to see little $t\bar{t}$ contribution. The results of this test, shown in Fig. 8, confirm that this ratio remains constant.

The D$\emptyset$ collaboration then applies the H_T and aplanarity cuts and uses the relative efficiency of these cuts on $t\bar{t}$ signal and the $W+$ jets background to extract the number of $t\bar{t}$ events in the sample and the number of background events that remain. The D$\emptyset$ collaboration estimates the size of the background in their $W+4$ jet sample to be 1.9 ± 0.5 events. There is a clear excess of observed events above the predicted background.

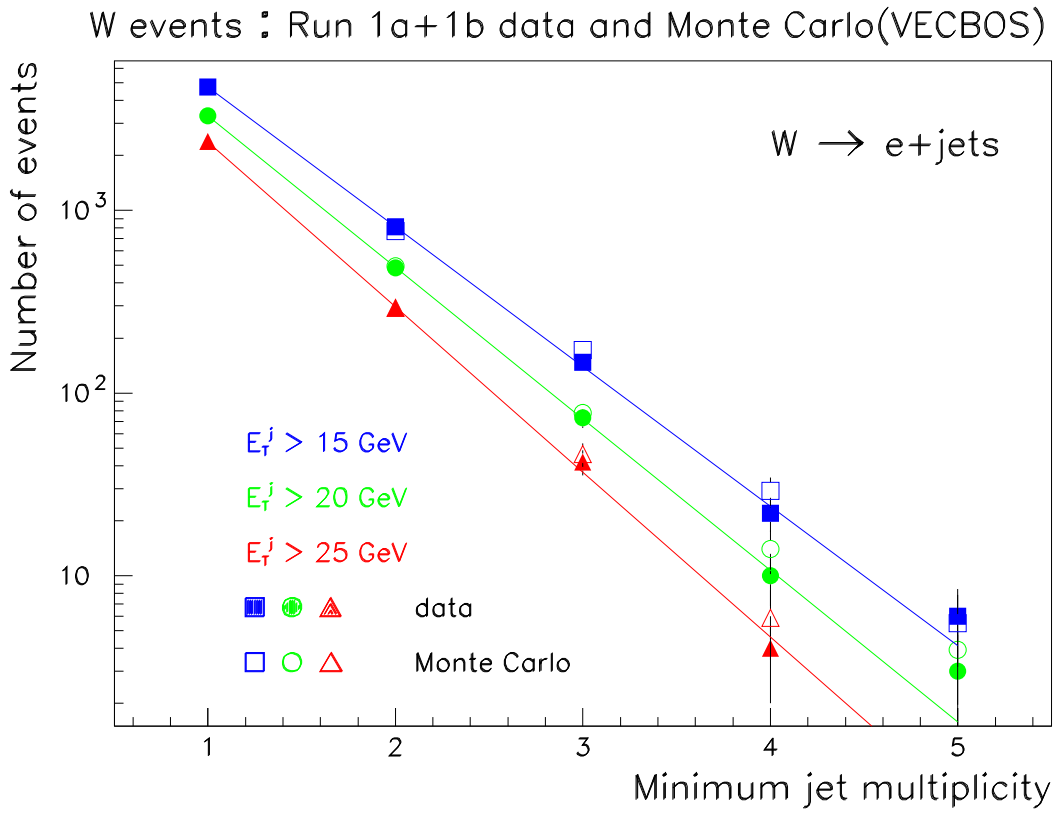

Figure 8: The rate of $W \to e\nu_e$ events as a function of the minimum jet multiplicity and jet E_T requirements observed by the DØ collaboration. These data are shown before the H_T or aplanarity cuts, and are compared to predictions from a QCD Monte Carlo calculation.

7.1.2 B Tagging in the DØ Sample

DØ has performed a separate analysis requiring that one of the jets also be consistent with a b quark semileptonic decay. This study is complementary to the DØ kinematical analysis, and does not depend on the jet-scaling arguments to estimate the backgrounds.

DØ's excellent muon identification capability makes it possible to tag b hadrons by searching for the decay $b \to \mu\nu_\mu X$. Because there are two b jets in each $t\bar{t}$ signal event, the fraction of tagged events will be twice the semileptonic branching fraction of b hadrons times the efficiency for identifying muons. DØ studies show that the use of standard muon identification requirements applied to candidates with $P_T >$ 4 GeV/c result in a tagging efficiency for $W+ \geq 3$ jet events of $\sim 20\%$. This is relatively insensitive to the actual top quark mass, rising slowly as a function of M_{top}.

"Fake" tags are expected to arise from real muons resulting from heavy quark (b, c) semileptonic decay and decays-in-flight of π and K mesons. This would imply that the fake rate per jet would remain relatively independent of the number of jets in a given event, or the topology of the jets in the event. The DØ collaboration has

measured the expected background rate for their tagging scheme using a large sample of events coming from their inclusive jet triggers. Since the jets in these events are expected to arise predominantly from light quarks and gluons, they form a good sample to estimate the probability of tagging a light quark or gluon jet as coming from a b quark. This leads to an over-estimate of the background from light quark jets, as some of the jets in this inclusive jet sample will have c and b quarks in them, albeit at a low rate. These studies show that the tag rate is between 0.005 and 0.010 per jet, and rises slowly with the E_T of the jet. Detailed Monte Carlo calculations using a full detector simulation verify this result. Based on this study, DØ expects that $\sim 2\%$ of the $W + 3$ or 4 jet background events will be tagged, with provides an order of magnitude improvement in signal-to-noise in this sample.

The DØ collaboration use a less stringent $W+$ jets selection when also requiring a b quark tag in order to optimise the signal-to-noise of this analysis. The events are required to have $H_T > 140$ GeV, and the jet multiplicity requirement is relaxed to demand ≥ 3 jets with $E_T > 20$ GeV. In addition, the aplanarity cut is dropped altogether, and in the case of the electron + jets channel, the $\not\!\!E_T$ cut is relaxed to require $\not\!\!E_T > 20$ GeV. There are 3 events in the e+jet and μ+jet channels that survive these requirements, whereas only 0.85 ± 0.14 and 0.36 ± 0.08 events are expected from background sources. As in the dilepton and lepton + jets channels, a excess of candidate events over background is observed.

7.2 The CDF Counting Experiment

The CDF collaboration has performed an analysis of their lepton + jets data similar to that reported for the Run 1A dataset [9]. The analysis avoids making stringent kinematical cuts that could result in large systematic uncertainties, and takes advantage of the presence of two b quarks in the signal events to control the expected backgrounds.

Starting from the inclusive W sample, the CDF analysis requires at least three jets with $E_T > 15$ GeV and $|\eta| < 2.0$. This results in 203 events, with 164 and 39 events in the $W + 3$ and $W+ \geq 4$ jet samples. The backgrounds estimated to make the largest contribution to this sample come from real $W^{\pm}$ boson production, from standard model sources of other isolated high E_T leptons (such as Z° production), from b and c quark semileptonic decays and from events where the lepton candidate has been misidentified. Most of the non-$W^{\pm}$ backgrounds have lower $\not\!\!E_T$, and are characterised by lepton candidates that are not well isolated from other particles in the event. The correlation between this additional energy flow and $\not\!\!E_T$ in the event allows one to directly measure this background fraction. This results in an estimate for the background from sources of non-isolated lepton candidates of $10 \pm 5\%$. The background rates from sources that produce isolated lepton candidates have been estimated using data and Monte Carlo calculations. These background estimates are summarised in Table 4.

Background	Fraction of Sample (%)
WW, WZ production	5.0 ± 2.3
$Z^\circ \to e^+e^-/\mu^+\mu^-$	5.2 ± 1.3
$Z^\circ \to \tau^+\tau^-$	3.3 ± 1.0
Fake leptons, conversions, $b\bar{b}$	10.0 ± 5.0
Total	23.5 ± 5.7

Table 4: The estimated fractions of events in the $W+ \geq 3$ jet sample arising from the different background sources to $t\,\overline{t}$ production. Only the requirement of ≥ 3 jets has been imposed.

7.2.1 Secondary Vertex Tagging

The CDF detector has the unique capability of detecting b quarks by reconstructing the location of the b quark's decay vertex using the SVX detector. A schematic of the decay topology for a bottom hadron is shown in Fig. 9. The charged particle trajectories are reconstructed in the CTC and then extrapolated into the SVX detector to identify the track's hits in the silicon strip detector.

The quality of the reconstructed SVX track is determined by the number of SVX coordinates found for the track and the quality of each coordinate. The algorithm to reconstruct secondary vertices considers all tracks above a transverse momentum of 1.5 GeV/c that have an impact parameter relative to the primary vertex $> 2\sigma$. The algorithm first looks for vertices formed by three tracks, making relatively loose quality cuts on each of the tracks. A vertex is accepted if a χ^2 fit requiring the three tracks to come from a common point is acceptable. Any remaining high-quality tracks with large impact parameter are then paired up to look for two-track vertices. A jet containing a secondary vertex found in this way that has a positive decay length is considered SVX tagged (the sign of the decay length is taken from the dot product of the displacement vector between the primary and secondary vertices and the vector sum of the momenta of the daughter tracks).

The efficiency of this SVX tagging algorithm has been measured using a large sample of inclusive electron and $J/\psi \to \mu^+\mu^-$ candidates, where the heavy quark contents in these samples have been independently estimated. This efficiency agrees with that obtained using a full detector simulation; the ratio of two estimates is 0.96 ± 0.07.

The b quark SVX tags not arising from $t\,\overline{t}$ production arise from track combinations that for some reason result in a fake secondary vertex (mistags), and from real sources of b and c quarks in $W+$ jet events. One way of estimating the mistag rate is to note that the rate of these fakes must be equal for those that fall in front of or behind the collision point (positive and negative tags, respectively). The rate of real b and c quarks not arising from $t\,\overline{t}$ production can be estimated using theoretical calculations

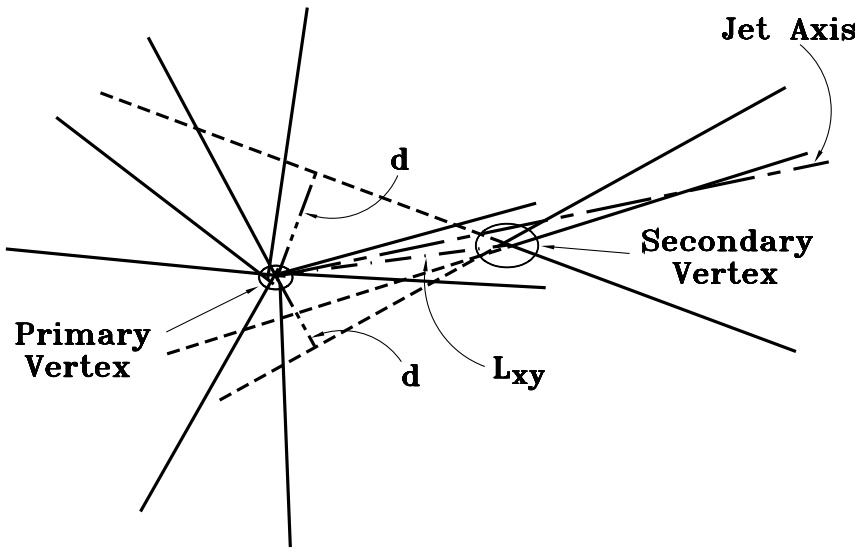

Figure 9: A schematic of the decay of a bottom quark, showing the primary and secondary vertices, and the charged tracks reconstructed in the CDF CTC and SVX detectors.

and comparing these with observed rates in other channels.

The mistag probability has been measured using both samples of inclusive jets and the inclusive electron and dimuon samples. The probability of mistagging, as a function of the number of jets in the event and the transverse energy of the jet is shown in Fig. 10, based on the inclusive jet measurements where we have plotted both the negative and positive tag rates. The negative tag rate is perhaps the best estimate of the mistag rate, since we expect some number of real heavy quark decays in this sample to enhance the positive tag rate. The mistag rate per jet measured in this way is ~ 0.008, and is lower than the positive tag rate measured in the inclusive jet sample (~ 0.025), as expected from estimates of heavy quark production in the inclusive jet sample.

To account for all sources of background tags, the number of tagged events expected from sources of real heavy quark decays (primarily $Wb\bar{b}$ and $Wc\bar{c}$ final states) is determined using a Monte Carlo calculation and a full simulation of the detector. The sum of this "physics" tag rate and the mistag rate then gives us an estimate of the total background to $t\bar{t}$ production. This estimate can be checked by using the positive tag rate in inclusive jet events as a measure of the total non-$t\bar{t}$ tag rate in the $W+$ jet events. This gives us a somewhat higher background rate, due primarily to the expected larger fraction of b and c quarks in the inclusive jet sample compared to the $W+$ jet events.

The efficiency for finding at least one jet with an SVX tag in a $t\bar{t}$ signal event is calculated using the ISAJET Monte Carlo programme [22] to generate a $t\bar{t}$ event, and then applying the measured tagging efficiencies as a function of jet E_T to the reconstructed b quark jets. The SVX tagging efficiency, *i.e.* the fraction of $t\bar{t}$ events with at least one SVX-tagged jet, is found to be 0.42 ± 0.05, making this technique

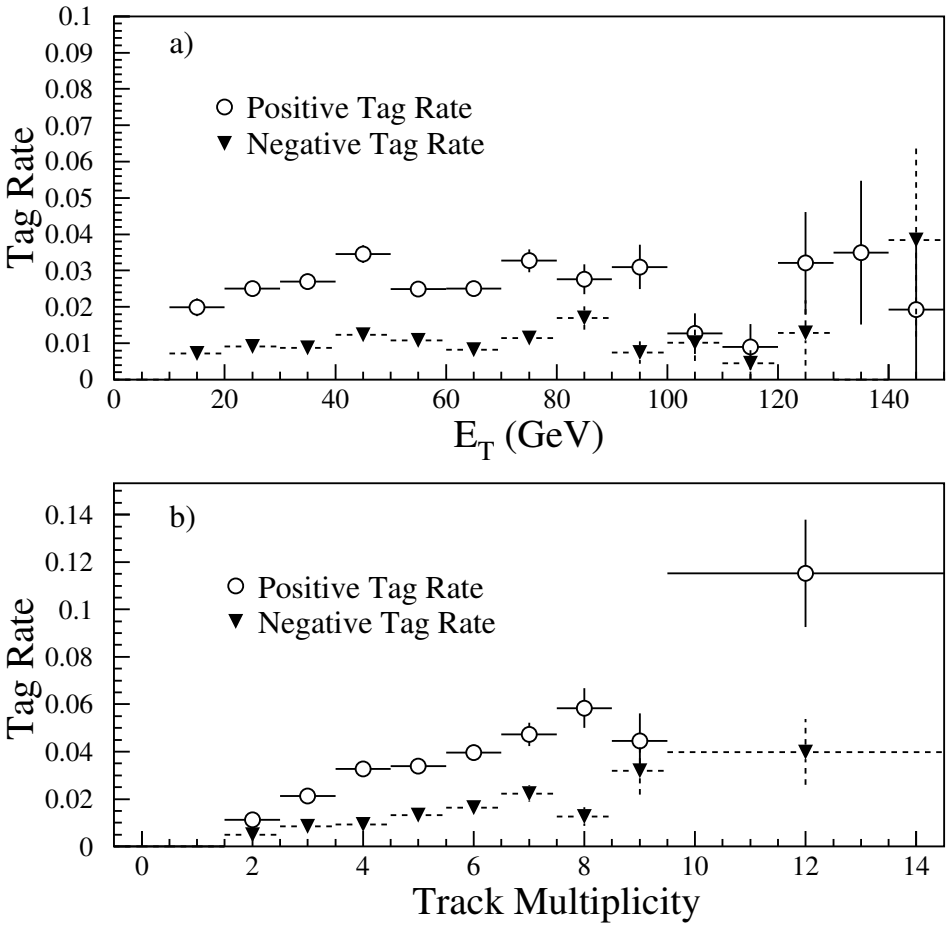

Figure 10: The rate of SVX tags as a function of the transverse energy of the jet and the charged track multiplicity in the jet, as measured using the inclusive jet sample. Tag rates for both positive and negative decay length vertices are shown.

a powerful way of identifying $t\,\overline{t}$ candidate events.

7.2.2 Soft Lepton Tagging

The CDF collaboration developed the original lepton-tagging techniques to search for $t\,\overline{t}$ production [23], requiring the presence of a muon candidate in proximity to one of the jets. The collaboration has enhanced these techniques by extending the acceptance of the muon system and by also searching for electron candidates associated with a jet cluster. In both cases, it is optimal to allow for relatively low energy leptons (down to P_T's as low as 2 GeV/c), so that this technique has become known as "soft lepton tagging." A candidate jet cluster with a soft lepton candidate is considered to be SLT tagged.

The efficiency of this tagging technique depends on the ability to identify leptons in the presence of additional hadrons that come from the fragmentation of the b quark and the decay of the resulting c quark system. Muons are identified by

requiring a charged track in the CTC that matches a muon track stub. Electron candidates are defined by an electromagnetic shower in the calorimeter with less than 10% additional energy in the hadronic calorimeter towers directly behind the shower, a well-reconstructed track in the CTC that matches the position of the shower, and shower profiles consistent with those created by an electron. The overall efficiency for finding at least one SLT tag in a $t\bar{t}$ event is 0.22 ± 0.02, and is not a strong function of the top quark mass.

The rate at which this algorithm misidentifies light quark or gluon jets as having a soft lepton is determined empirically by studying events collected by requiring the presence of at least one jet cluster. The mistag rate for muon tags varies between 0.005 and 0.01 per charged track, and rises slowly with the energy of the jet. The mistag rate for electrons also depends on the track momentum and how well isolated it is from other charged tracks; it typically is of order 0.005 per track. Fake SLT tags where there is no heavy flavour semileptonic decay is expected to be the dominant source of background tags in the $t\bar{t}$ sample, due to the larger SLT fake rates as compared to the SVX mistag rates.

7.2.3 Tagging Results in the CDF Lepton+Jets Sample

The SVX and SLT tagging techniques have been applied to the W+jet sample as a function of the number of jets in the event, and the expected number of mistags has been calculated for each sample. This provides a very strong consistency check, as the number of observed tags in the $W + 1$ jet and $W + 2$ jet samples should be dominated by background tags; the fraction in these two event classes expected from $t\bar{t}$ production is less than 10% of the total number of candidate events.

The number of candidate events and tags is shown in Table 5. There is good agreement between the expected number of background tags and the number of observed tags for the $W + 1$ jet and $W + 2$ jet samples. However, there is a clear excess of tags observed in the $W+ \geq 3$ jet sample, where we observe 27 and 23 SVX and SLT events, respectively, and expect only 6.7 ± 2.1 and 15.4 ± 2.3 SVX and SLT background tags. The excess of SVX tags is particularly significant, with the probability of at least this number of tags arising from background sources being 2×10^{-5}. The excess of SLT tags is less significant because of the larger expected background. The probability that at least 23 observed SLT tags would arise from background only is 6×10^{-2} and confirms the SVX observation.

It is interesting to note that if we attribute the excess number of SVX tags in the $W+ \geq 3$ jet sample to $t\bar{t}$ production, we would expect approximately 10 $W + 2$ jet tagged events resulting from $t\bar{t}$ production. This is in good agreement with the excess of observed tags (13 ± 7) in this sample, and corroborates the hypothesis that the excess in the $W+ \geq 3$ jet sample is due to the $t\bar{t}$ process.

A striking feature of the tagged sample is the number of events with two or more tagged jets. The 27 SVX tags are found in 21 events, so that there are 6 SVX double tags. There are also six SVX tagged events that have SLT tags. We would expect

Sample	SVX bkg	SVX tags	SLT bkg	SLT tags
W+1 jet	50 ± 12	40	159 ± 25	163
W+2 jet	21 ± 7	34	46 ± 7	55
W+$\geq$ 3 jet	6.7 ± 2.1	27	15.4 ± 2.3	23

Table 5: The expected number of background tags and the observed number of tags in the CDF lepton+jets sample as a function of the number of jets in event.

Sample	Background	Observed
CDF Dileptons	1.3 ± 0.3	6
D$\emptyset$ Dileptons	0.65 ± 0.15	3
Lepton + Jets (D$\emptyset$ Kinematics)	0.93 ± 0.50	8
Lepton + Jets (D$\emptyset$ B Tagging)	1.21 ± 0.26	6
Lepton + Jets (CDF SVX tags)	6.7 ± 2.1	27
Lepton + Jets (CDF SLT tags)	15.4 ± 2.3	23

Table 6: The expected number of background events and the observed number of events in the different analyses. Note that some event samples and background uncertainties are correlated so it is not straightforward to combine these observations into a single statement of statistical significance.

less than one SVX-SVX double tag and one SVX-SLT double tag in the absence of $t\,\overline{t}$ production, whereas we would expect four events in each category using the excess of SVX tags to estimate the $t\,\overline{t}$ production cross section. These observations strengthen the $t\,\overline{t}$ interpretation of the CDF sample.

7.3 Summary of Counting Experiments

The results of the lepton+jets counting experiments performed by D$\emptyset$ and CDF are summarised in Table 6. Both collaborations observe an excess of events in all the channels in which one can reasonably expect evidence for the top quark. Many of the channels demonstrate correlated production of $W^{\pm}$ bosons with b quarks – exactly what we would expect from $t\,\overline{t}$ decay.

Taken together, this is overwhelming evidence that the two collaborations are observing phenomena that within the context of the standard model can only be attributed to pair production of top quarks.

8 Measurement of Top Quark Properties

In order to further test the interpretation that top quark production is responsible for the excess in the dilepton and lepton + jets channels, both collaborations have

measured the rate of top quark production and identified a subset of their candidate lepton+jet events where it is possible to directly measure the mass of the top quark.

These measurements allow us to test the standard model prediction for the cross section as a function of the top quark mass. The initial evidence for top quark production published by CDF [9] implied a top quark production cross section almost two standard deviations above the theoretically predicted value. Moreover, other standard model measurements, and in particular those performed at LEP, constrain the top quark mass. It is important to directly verify that these predictions agree with the top quark mass inferred from the Collider data.

8.1 The $t\bar{t}$ Cross Section

The acceptance of the DØ and CDF top quark searches depend on the top quark mass. We can therefore infer the $t\bar{t}$ production cross section as a function of the top quark mass given the number of observed events in each channel.

If we observe N_i^o candidate events in a particular channel i, with an acceptance ϵ_i, with N_i^b expected background events in a data sample with integrated luminosity $\mathcal{L}$, then the maximum likelihood solution for the cross section of the process is

$$\sigma = \frac{\sum_i \left(N_i^o - N_i^b\right)}{\mathcal{L}\left(\sum_i \epsilon_i\right)}. \tag{15}$$

This assumes that the observed number of events has a Poisson distribution and that uncertainties on the acceptance can be ignored. The latter restriction can be relaxed by numerically solving for the maximum likelihood solution allowing for uncertainties in ϵ_i and N_i^b, and any correlations in the acceptances.

The CDF collaboration has performed a preliminary measurement of the $t\bar{t}$ cross section using the SVX tagged sample. This is the single most significant measurement and can be performed only knowing the SVX tagging efficiency and background rates. The addition of the SLT sample and the dileptons into the cross section measurement requires a knowledge of the efficiency correlations in the samples and is work in progress. The $t\bar{t}$ acceptance was determined using the ISAJET Monte Carlo programme, and found to be 0.034 ± 0.009. The uncertainties associated with this acceptance calculation are listed in Table 7. The expected background in the 21 tagged events is $N^b = 5.5 \pm 1.8$ events[3]

The resulting cross section determined from the SVX sample is $6.8^{+3.6}_{-2.4}$ pb for a nominal top quark mass of 175 GeV/c^2. This is approximately one standard deviation lower than the cross section determined in the Run 1A CDF data. It is in good agreement with the theoretically predicted value of 4.9 ± 0.6 pb for the same top quark mass.

The DØ collaboration estimates the $t\bar{t}$ cross section using the information from all the channels. They also perform a background subtraction and then correct for the

[3]The previous estimate of the expected SVX background tags assumed that there was no contribution from $t\bar{t}$ production to the 203 events in the $W+ \geq 3$ jet sample prior to tagging.

Source	Uncertainty (%)
Lepton ID and Trigger	10
Initial State Radiation	7
Jet Energy Scale	6.5
B tagging Efficiency	12

Table 7: The uncertainties in the acceptance calculation for the CDF cross section measurement using the SVX tagged sample.

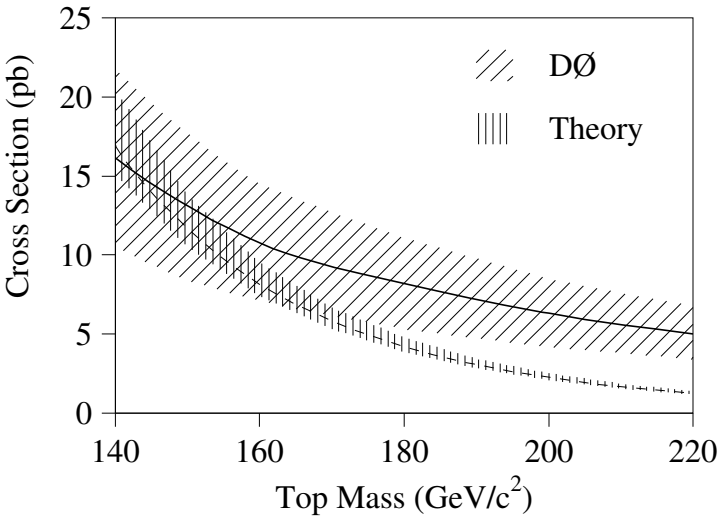

Figure 11: The top quark cross section determined by the DØ collaboration as a function of top quark mass. The QCD prediction for $t\bar{t}$ production is displayed as the heavier band.

acceptance, channel by channel. They determine $\sigma_{t\bar{t}} = 6.2 \pm 2.2$ pb, for a top quark mass of 200 GeV/c^2. This value doubles to ~ 12 pb if one assumes a top quark mass of 160 GeV/c^2. The top quark mass dependence of the DØ cross section is illustrated in Fig. 11.

The CDF and DØ estimates are in good agreement with each other, although both have large uncertainties. A strong test of the lowest order calculation for $\sigma_{t\bar{t}}$ and next-to-leading order corrections will have to wait for substantially more statistics.

8.2 The Top Quark Mass

The top quark mass can be determined directly by correlating the kinematics of the observed partons in the final state. The sensitivity of this measurement depends on the amount of "missing" information in the events, and the inherent resolution of the detectors to jets and missing energy. The lepton + ≥ 4 jet events offer the possibility of fully reconstructing the $t\bar{t}$ system provided one assumes that the missing

transverse energy arises from the undetected neutrino, and that four of the jets come from the b and $\bar{b}$ quarks and the two quarks from the $W^{\pm}$ decay.

Perhaps the most serious complication to this procedure is the difficulty of associating final state jet clusters with the partons from the $t\,\overline{t}$ decay. The jets are only approximate measures of the initial state parton, and there is often not a 1-to-1 correspondence between partons resulting from the $t\,\overline{t}$ decay and observed jets. This is due to gluon radiation that can cause one parton to be observed as two jet clusters, and overlap of jet clusters, where two partons merge into a single jet cluster. To complicate matters further, additional partons are produced by initial and final state radiation, so the number of observed jet clusters may readily exceed four.

The number of combinatorial possibilities for assigning partons to jets in the case where only four jets are observed is 12 (we only have to identify the two jets associated with the $W^{\pm}$ decay and not have to permute these two). If we can identify one of the jets as arising from a bottom quark, the number of possible assignments reduces to six. Any technique that reconstructs the $t\,\overline{t}$ decay in this mode has to reduce the effect of these combinatorial backgrounds on the expected signal.

8.2.1 CDF Mass Analysis

The CDF collaboration measures the top quark mass by selecting a sample of lepton+jet events with at least four jets, and then making the parton-jet assignment that best satisfies a constrained kinematic fit. The fit inputs are the observed jet momentum vectors, the momentum vector for the charged lepton, the transverse energy vector for the neutrino and the vector sum of the momentum of the unassigned jets in the event. The uncertainties in these quantities are determined from the measured response of the detector. The fit assumes that the event arises from the process

$$\begin{aligned} p\bar{p} \;\rightarrow\; & t\bar{t}X, \\ & \quad \hookrightarrow q\bar{q}'\,\bar{b} \\ & \quad \hookrightarrow l^{+}\nu_{l}\,b \end{aligned} \tag{16}$$

The fit constrains the $W^{\pm}$ decay daughters to have an invariant mass equal to the $W^{\pm}$ mass and constrains the t and the $\bar{t}$ to have the same mass. The unknown recoil system X is observed in the detector as unassociated jets and the "unclustered" energy in the calorimeter, *i.e.* the energy not associated with a jet. Only the four highest E_T jets are considered, reducing the possible combinations at the cost of some degradation in top quark mass resolution (in those cases where the $t\,\overline{t}$ daughter jets are not the four highest E_T jets in the event).

Formally, there are two degrees of freedom in the fit when we take into account the number of constraints and the number of unmeasured quantities. A χ^2 function including the uncertainties in the measurements is minimised subject to the kinematic constraints for each possible parton-jet assignment. The b-tagged jets in the event

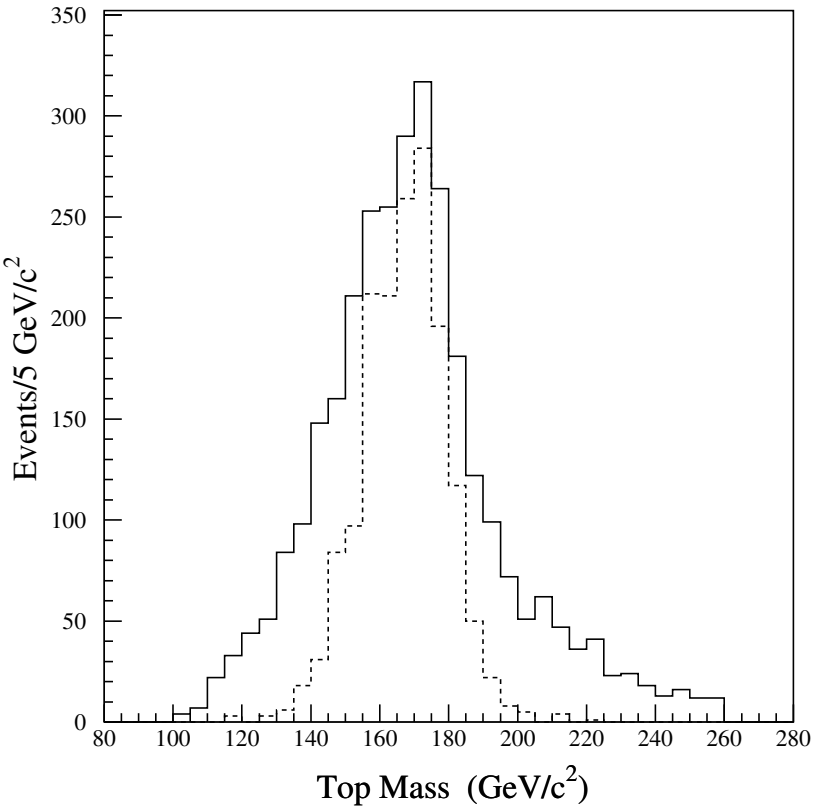

Figure 12: The fitted top quark mass in Monte Carlo events for those events in which the correct parton assignments have been made (dashed histogram) and for all events that pass the fit procedure (solid histogram). A top quark mass of 170 GeV/c^2 has been assumed.

are only allowed to be assigned to the b or $\bar{b}$ quarks. Prior to the fit all jet energies are corrected in order to account for detector inhomogeneities and the effect of energy flow into and out of the jet clustering cone. The parton assignment that produces the lowest χ^2 is selected for the subsequent analysis. The event is rejected if the minimum χ^2 is greater than 10. Parton assignments that result in a top quark mass greater than 260 GeV/c^2 are rejected as the experiment is not expected to have any sensitivity to top quark masses of that magnitude.

Monte Carlo studies have demonstrated that this procedure identifies the correct parton-jet assignment about 40% of the time. The top quark mass resulting from the fit in those cases is shown in Fig. 12 along with the mass distribution for all lepton + ≥ 4 jet events for a sample created assuming a top quark mass of 170 GeV/c^2. From a single event, we are able to measure the top quark mass to an accuracy of $\sim$ 10 GeV/c^2 when one makes the correct assignment. One also sees that the fitting and parton assignment procedure retains much of this mass information, even in those cases where the incorrect parton assignment has been made.

Starting with the 203 $W+ \geq 3$ jet events, the CDF collaboration selects a subset of events that have at least one additional jet with $E_T > 8$ GeV and $|\eta| < 2.4$. The

requirements on the fourth jet are less stringent than the first three jets in order to enhance the efficiency for detecting all four jets from the $t\bar{t}$ decay. There are 99 such events in the CDF sample prior to requiring a b-tagged jet, and 88 of these pass the χ^2 cut on the best jet-parton assignment and kinematic fit. The additional requirement of at least one SVX or SLT-tagged jet leaves 19 events.

The background of non-$t\bar{t}$ events in this sample is estimated in the same manner used in the cross section analysis. One assumes that the 88 event sample is a mixture of background and $t\bar{t}$ signal, and then applies the known background tag rates to determine how many of the non-$t\bar{t}$ events would be tagged. This results in a estimated background in the 19 events of $6.9^{+2.5}_{-1.9}$ events. This background is expected to be a combination of real W+jet events and events where an energetic hadron fakes the lepton signature. Studies of the Z+jet events, candidate events where the lepton is not well-isolated, and W+jet Monte Carlo events show that the resulting top quark mass distribution for these different background events are all similar. The CDF collaboration therefore uses the W+jets Monte Carlo sample to estimate the background shape in the top quark mass distribution.

The resulting top quark mass distribution is shown in Fig. 13. One sees a clear peak around 170-180 GeV/c^2 with relatively long tails. The dotted distribution represents the shape of the non-$t\bar{t}$ backgrounds, normalised to the estimated background rate. The top quark mass is determined by performing a maximum likelihood fit of this distribution to a linear combination of the expected $t\bar{t}$ signal shape determined by Monte Carlo calculations for different top quark masses and the background. The background rate is constrained by the measured rate of non-$t\bar{t}$ events in the sample. The negative log-likelihood distribution for this fit is shown in the inset in Fig. 13. It results in a top quark mass of 176 ± 8 GeV/c^2.

The largest systematic uncertainties in this measurement arise from uncertainties in the modelling of gluon radiation in jets in the final state, absolute jet energy scale, variations in fitting procedures, and the shape of the non-$t\bar{t}$ background. A number of other potential sources of uncertainty have been studied, and have been found to contribute a total of 2.0 GeV/c^2 to the total systematic uncertainty. A summary of these uncertainties is given in Table 8, and total to ± 10 GeV/c^2.

One can quantify the significance of the shape of the mass distribution by performing an unbinned Kolmogorov-Smirnov test. The probability that the observed mass distribution could arise from purely background sources is 2×10^{-2}. This test is conservative in that it only compares the shape of the background with the observed data. Other measures of significance can be used. For example, one can define a relative likelihood for the top+background and background-only hypotheses and then ask how often a background-only hypothesis would result in a relative likelihood as significant as that observed. This test gives a probability for a background fluctuation of less than 10^{-3}. However, it is more model-dependent as it assumes a specific shape for the non-background hypothesis.

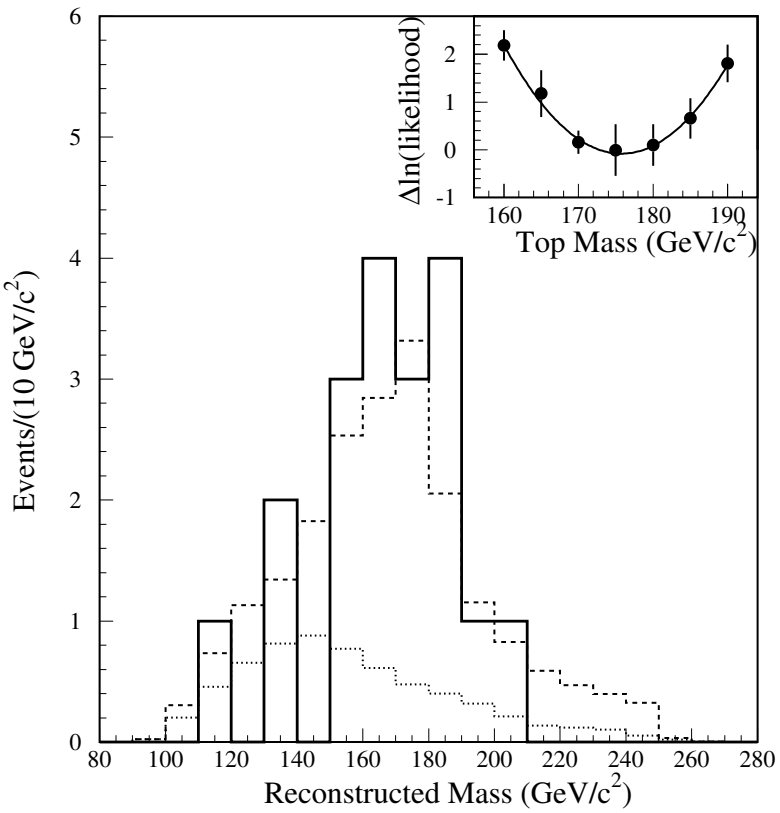

Figure 13: The fitted top quark mass for the 19 events in the CDF sample with four or more jets that satisfy the fit criteria. The dotted histogram reflects the shape and size of the estimated background. The dashed histogram is the result of a fit of the reconstructed mass distribution to a combination of $t\,\overline{t}$ signal and expected background. The inset distribution is the change in log-likelihood of this fit.

Source	Uncertainty (GeV/c^2)
Final State Gluon Radiation	7.7
Absolute Jet Energy Scale	3.1
Variations in Fit Procedures	2.5
Shifts Resulting from Tagging Biases	2.4
Monte Carlo statistics	3.1
Non-$t\,\overline{t}$ Mass Distribution Shape	1.6
Miscellaneous effects	2.0

Table 8: The systematic uncertainties associated with the CDF top quark mass measurement.

8.2.2 The DØ Mass Measurement

The DØ collaboration estimates the top quark mass using their sample of lepton + ≥ 4 jet events. In their analysis, they select 4-jet events by requiring that all jets have a corrected transverse energy > 15 GeV with $|\eta| < 2.4$. They also require the events to have $H_T > 200$ GeV and to have aplanarity > 0.05. They find 14 events that satisfy these requirements.

They then perform a χ^2 fit of the observed kinematics in each event to the $t\bar{t} \rightarrow W^+W^-b\bar{b}$ hypothesis, requiring that the mass of the assumed $t \rightarrow l\nu_l b$ system equal the mass of the $t \rightarrow q\bar{q}b$ system making all possible parton-jet assignments in the final state. As in the CDF technique, they only consider the four highest E_T jets, and only fits with $\chi^2 < 7$ are considered acceptable. There are 11 events that have at least one configuration that gives an acceptable fit. For each event, they assign a top quark mass by averaging the top quark mass from the three best acceptable fits for that event, weighting the mass from each fit with the χ^2 probability from the fit. The resulting histogram of the invariant mass of the three-parton final state (the hypothesised top quark) is shown in Fig. 14(a). They performed the same analysis on a "looser" data sample of 27 events, where the H_T and aplanarity requirements were removed. This yielded similar results, as shown in Fig. 14(b), although with significantly larger backgrounds. The mass distribution shows an enhancement at a three-parton invariant mass around 200 GeV/c^2, as expected from $t\,\overline{t}$ production (shown as the higher mass curve in both plots). The corresponding mass distribution expected from the QCD $W+$ jet background is shown in Fig. 14(a)-(b) as the dashed curve at lower mass. It peaks at small values of three-parton invariant mass and together the combined background and signal hypothesis model the data well.

The mass distribution obtained using the looser selection is fit to a combination of $t\,\overline{t}$ signal and background, yielding a top quark mass of

$$M_{\rm top} = 199^{+19}_{-21} \pm 22 \text{ GeV/c}^2, \tag{17}$$

where the two uncertainties are statistical and systematic, respectively. A similar fit to the mass distribution using the 11 event sample results in a consistent result, but with larger statistical uncertainties. The negative log-likelihood distributions for the fits to the standard and loose selection are shown in Fig. 14(c) and (d), respectively. The systematic uncertainty is dominated by the sensitivity of this analysis to the DØ jet energy scale.

9 Future Work

The observation and study of the top quark is currently statistics limited. Both the DØ and CDF collaborations are accumulating additional data at the Collider. By the end or Run 1, currently scheduled for the February 1996, both collaborations expect to at least double their datasets. This will improve both the statistical uncertainties

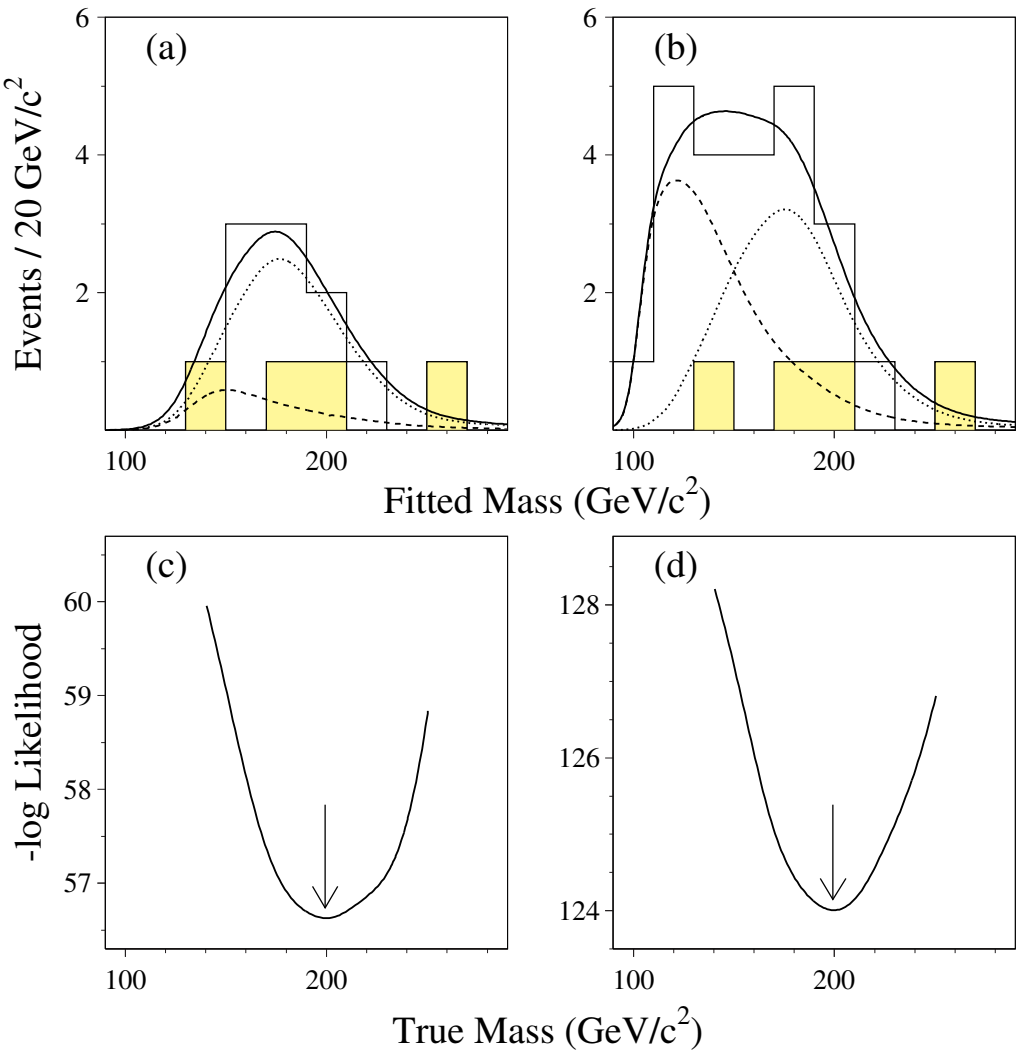

Figure 14: The distribution of the three-jet invariant mass versus the top quark mass obtained from the DØ lepton + 4 jet sample. Figures a) and b) show the results of the standard and "loose" selection, respectively. Figures c) and d) show the likelihood distribution for fits of the mass distributions to a combination of signal and background terms.

on the top quark cross section and mass, and will simultaneously allow additional studies that will help to reduce the systematic uncertainties in these measurements.

The top quark system is itself a probe into the physics of the standard model. With the anticipated size of the Tevatron data samples, it will be possible to measure the branching fraction $t \to W^+ b$, which is expected to saturate the top quark width, and place constraints on other decay modes such as $t \to b\tau\nu_\tau$. The top quark is also a probe into physics beyond the standard model [24]. A number of theoretical extensions to the standard model can be tested by detailed studies of the $t\bar{t}$ system.

10 Conclusions

The CDF and DØ collaborations have recently published data that confirms the existence of the sixth flavour of quark in the standard model, the top quark. The preliminary estimates of its mass, $176 \pm 10 \pm 13$ GeV/c^2 (CDF) and $199^{+19}_{-21} \pm 22$ GeV/c^2 (DØ) make it the heaviest known fermion in the standard model. The observed rate of $t\bar{t}$ events is consistent with standard model predictions, and make it the rarest phenomena observed in proton-antiproton annihilations.

The data used to confirm the top quark's existence comprise only half of the total dataset that is expected to be available within a year's time. It is therefore reasonable to expect rapid progress on the measurement of more detailed properties of the top quark. Because of the massiveness of this fermion, it will be a unique probe into the physics of the standard model and what lies beyond this theory.

Acknowlegements

I would like to thank the members of the DØ and CDF collaborations who kindly provided me with details of their respective analyses. I would also like to note that the research reported here would not have been successful without the excellent support of the staff of the Fermilab National Accelerator Laboratory and the institutions involved in this research.

Support for this work from the National Sciences and Engineering Research Council of Canada is gratefully acknowledged.

References

1. S. W. Herb *et al.*, Phys. Rev. Lett. **39**, 352 (1977).
2. R. Keeler, these proceedings.
3. R. Ammar *et al.* (CLEO Collaboration), Phys. Rev. **D49**, 5701 (1994).
4. Review of Particle Properties, Phys. Rev. **D50**, 1304 (1994).
5. D. Decamp *et al.* (ALEPH Collaboration), Phys. Lett. **B236**, 511 (1990);
   O. Adriani *et al.* (L3 Collaboration), Phys. Lett. **B313**, 326 (1993);
   P. Abreu *et al.* (DELPHI Collaboration), Phys. Lett. **B242**, 536 (1990);
   M. Z. Akrawy *et al.* (OPAL Collaboration), Phys. Lett. **B236**, 364 (1990);
   G. S. Abrams *et al.* (MARK II Collaboration), Phys. Rev. Lett. **63**, 2447 (1989);
   I. Adachi *et al.* (TOPAZ Collaboration), Phys. Lett. **B229**, 427 (1989);
   S. Eno *et al.* (AMY Collaboration), Phys. Rev. Lett. **63**, 1910 (1989);
   H. Yoshida *et al.* (VENUS Collaboration), Phys. Lett. **B198**, 570 (1987).
6. F. Abe *et al.* (CDF Collaboration), Phys. Rev. Lett. **74**, 341 (1995);
   F. Abe *et al.* (CDF Collaboration), Phys. Rev. Lett. **73**, 220 (1994);
   C. Albajar *et al.* (UA1 Collaboration), Phys. Lett. **B253**, 503 (1991);
   J. Alitti *et al.* (UA2 Collaboration), Phys. Lett. **B276**, 365 (1991).
7. F. Abe *et al.* (CDF Collaboration), Phys. Rev. Lett. **73**, 2667 (1994).

8. S. Abachi *et al.* (DØ Collaboration), Phys. Rev. Lett. **72**, 2138 (1994).
9. F. Abe *et al.* (CDF Collaboration), Phys. Rev. Lett. **73**, 225 (1994); Phys. Rev. **D50**, 2966 (1994).
10. F. Abe *et al.* (CDF Collaboration), Phys. Rev. Lett. **74**, 2626 (1995); S. Abachi *et al.* (DØ Collaboration), Phys.Rev. Lett. **74**, 2632 (1995).
11. P. Nason, S. Dawson and R. K. Ellis, Nucl. Phys. **B303**, 607 (1988); W. Beenakker, H. Kuijf and W. L. van Nerven, Phys. Rev. **D40**, 54 (1989); G. Altarelli, M. Diemoz, G. Martinelli and P. Nason, Nucl. Phys. **B308**, 724 (1988).
12. E. Laenen, J. Smith and W. L. van Neerven, Nucl. Phys. **B369**, 543 (1992); E. Laenen, J. Smith and W. L. van Neerven, Phys. Lett. **321B**, 254 (1994).
13. S. Frixione, M. Mangano, P. Nason and G. Ridolfi, Phys. Lett. **B351**, 555 (1995).
14. F. A. Berends, W. T. Giele, H. Kuijf and B. Tausk, Nucl. Phys. **B357**, 32 (1991).
15. F. Abe *et al.* (CDF Collaboration), Phys. Rev. Lett. **70**, 4042 (1993).
16. S. Abachi *et al.* (DØ Collaboration), Nucl. Instrum. Methods **A350**, 73 (1994).
17. F. Abe *et al.* (CDF Collaboration), Nucl. Instrum. Methods Phys. Res. A **271**, 387 (1988).
18. Details of the CDF and DØ jet cluster algorithms are provided in: F. Abe *et al.* (CDF Collaboration), Phys. Rev. **D45**, 1448 (1992). S. Abachi *et al.* (DØ Collaboration), FERMILAB-PUB-95-020-E, July 1995, submitted to Phys. Rev. **D**.
19. F. Abe *et al.* (CDF Collaboration), FERMILAB-PUB-95-149-E, June 1995. Submitted to Phys. Rev. Lett.
20. See, for example, V. D. Barger and R. J. N. Phillips, "Collider Physics," Addison-Wesley Publishing Co. (1987), p. 281.
21. Review of Particle Properties, Phys. Rev. **D50**, 1278 (1994).
22. F. Paige and S. D. Protopopescu, BNL Report No. 38034, 1986 (unpublished).
23. F. Abe *et al.* (CDF Collaboration), Phys. Rev. Lett. **68**, 447 (1992); Phys. Rev. **D45**, 3921 (1992).
24. See, for example, C. T. Hill, Phys. Lett. **B345**, 483 (1995); B. Holdom and M. V. Ramana, Phys. Lett. **B353**, 295 (1995).